JOURNAL OF ENZYME INHIBITION AND MEDICINAL CHEMISTRY
2021, VOL. 36, NO. 1, 627–639
https://doi.org/10.1080/14756366.2021.1882452

Taylor & Francis
Taylor & Francis Group

RESEARCH PAPER

New 3-*O*-substituted xanthone derivatives as promising acetylcholinesterase inhibitors

Zi Han Loh[a], Huey Chong Kwong[b], Kok Wai Lam[c], Soek Sin Teh[d], Gwendoline Cheng Lian Ee[e], Ching Kheng Quah[f], Anthony Siong Hock Ho[a] and Siau Hui Mah[a,g]

[a]School of Biosciences, Taylor's University, Lakeside Campus, Subang Jaya, Malaysia; [b]School of Chemical Sciences, Universiti Sains Malaysia, George Town, Malaysia; [c]Drug and Herbal Research Centre, Faculty of Pharmacy, Universiti Kebangsaan Malaysia, Kuala Lumpur, Malaysia; [d]Energy and Environment Unit, Engineering and Processing Division, Malaysian Palm Oil Board, Bandar Baru Bangi, Malaysia; [e]Department of Chemistry, Faculty of Science, University Putra Malaysia, Serdang, Malaysia; [f]X-ray Crystallography Unit, School of Physics, Universiti Sains Malaysia, George Town, Malaysia; [g]Centre for Drug Discovery and Molecular Pharmacology, Faculty of Health and Medical Sciences, Taylor's University, Lakeside Campus

ABSTRACT

A new series of 3-*O*-substituted xanthone derivatives were synthesised and evaluated for their anti-cholinergic activities against acetylcholinesterase (AChE) and butyrylcholinesterase (BChE). The results indicated that the xanthone derivatives possessed good AChE inhibitory activity with eleven of them (**5**, **8**, **11**, **17**, **19**, **21**-**23**, **26**-**28**) exhibited significant effects with the IC_{50} values ranged 0.88 to 1.28 μM. The AChE enzyme kinetic study of 3-(4-phenylbutoxy)-9*H*-xanthen-9-one (**23**) and ethyl 2-((9-oxo-9*H*-xanthen-3-yl)oxy)acetate (**28**) showed a mixed inhibition mechanism. Molecular docking study showed that **23** binds to the active site of AChE and interacts via extensive π–π stacking with the indole and phenol side chains of Trp86 and Tyr337, besides the hydrogen bonding with the hydration site and π–π interaction with the phenol side chain of Y72. This study revealed that 3-*O*-alkoxyl substituted xanthone derivatives are potential lead structures, especially **23** and **28** which can be further developed into potent AChE inhibitors.

ARTICLE HISTORY
Received 21 September 2020
Revised 16 December 2020
Accepted 20 January 2021

KEYWORDS
Alzheimer's disease; enzyme kinetic study; molecular docking; synthesis; structure–activity relationship study

Introduction

Dementia is a syndrome of deterioration in memory, thinking, orientation, comprehension, calculation, learning capacity, language, judgement, and the ability to perform daily activities. An estimated number of 50 million people worldwide are living with dementia and the number is speculated to rise to 75 million in 2030 and 131.5 million in 2050 due to an increase of the aged population[1]. Furthermore, the current costs associated with dementia are tremendous with approximately 1 trillion US dollars and it is estimated to rise to 2 trillion US dollars by year 2030[1]. Alzheimer's disease (AD) was reported to account for 60–80% of all cases of dementia, besides Lewy body dementia, frontotemporal disorders and vascular dementia in 2019 Alzheimer's disease facts and figures report[2]. AD is commonly affecting the elderly as the occurrence of AD doubles every five years beyond the age of 65. It is an irreversible and progressing neurodegenerative brain disorder that leads to cognitive impairment and memory loss[3]. AD is a very burdensome disease to patients and their families, as well as informal caregivers, due to long term illness in terms of disability and dependence[4]. Therefore, AD becomes one of the biggest global health challenges for society.

The pathogenesis of AD is multifactor, including the loss of cholinergic neuron, extracellular deposit of fibrils, aggregation of amyloid beta-peptide, oxidative stress, neuroinflammation. The most well-received hypothesis is the deficit of an important neurotransmitter in the cholinergic neurotransmission, acetylcholine (ACh)[3,5–7]. The deficit of ACh has profound effects on the signaling that involves learning ability and long-term memory[8–10]. The cholinesterase enzymes, acetylcholinesterase (AChE) and butyrylcholinesterase (BChE) are accountable for the degradation of ACh through hydrolysis. Thus, cholinesterase inhibitors are important drugs in treating AD by maintaining the level of ACh[10–12]. AChE predominates in the brain of a healthy person and contributes to ACh hydrolysis in the brain for approximately 80%[7,13]. Studies have shown that the inhibition of AChE could prevent the degradation of ACh and in turn sustaining its level and duration of action[14,15]. Furthermore, AChE could facilitate the formation of amyloid fibril to obtain a stable AChE-β-amyloid complex, which is more toxic than single β-amyloid peptides[5]. Hence, targeting AChE could hinder the production of AChE-β-amyloid complexes. The current management of AD is focussing on the enhancement of the concentration of ACh in the synaptic cleft by inhibiting cholinesterase[16,17]. Most of the U.S. Food and Drug Administration (FDA)-approved prescription drugs for AD are AChE inhibitors including Donepezil[18], Galanthamine[19], and the dual cholinesterase inhibitor Rivastigmine[20]. Moreover, patients who received treatment with AChE inhibitor experienced a deceleration of the progression of the disease and an increase of attention span[21]. Therefore, research studies on the discovery and development of AChE inhibitors with higher potency and efficacy

CONTACT Siau Hui Mah siauhui.mah@taylors.edu.my School of Biosciences, Taylor's University, Lakeside Campus, 1, Jalan Taylor's, 47500 Subang Jaya, Selangor, Malaysia

Supplemental data for this article can be accessed here.

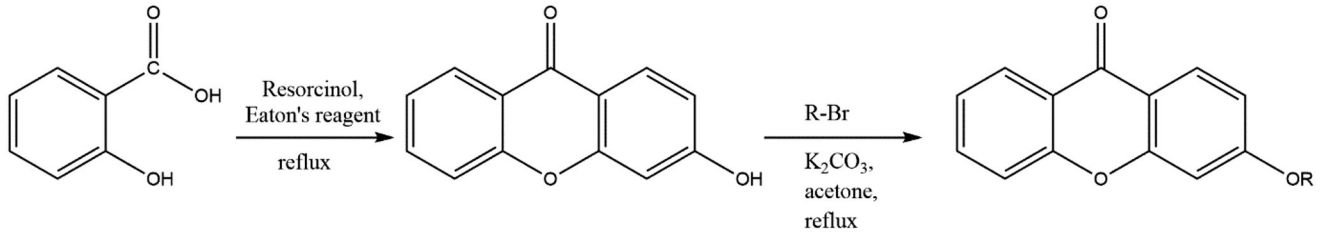

Figure 1. Reaction scheme for the synthesis of xanthone derivatives.

is essential since these inhibitors are the therapeutically potential as a principal approach of AD treatments. The adverse effects were associated with currently available drugs and worse still that there is no cure for AD up to date. Current approaches for the treatment of AD are solely focussing on maintaining the mental function, managing behavioural symptoms, and slowing down or delaying the symptoms of the disease[22]. Hence, this study aimed to search for lead compounds with significant cholinesterase inhibitory activities that are highly potential to be further developed into alternative drugs to treat AD more effectively.

To date, more than 50% of the marketed drugs were developed from natural products, especially secondary metabolites and their derivatives[23,24]. Xanthones are one of these important secondary metabolites that possessed a broad spectrum of biological activities such as anti-cancer[25], antioxidant[26], antibacterial[27], antifungal[28], antimalarial[29], antidiabetic[30,31], anti-cholinergic[15,32] and anti-inflammatory activities[33–36]. The biological activities of xanthones vary depending on their chemical structures, particularly the type of substituents and their respective positions on the two phenyl rings of the core structure of xanthone[37–39]. However, xanthones obtained from the natural resources are limited in substituent variation available on the rings[37], as well as time-consuming on the extraction and purification processes[40]. Hence, structural modification of xanthone-based skeleton is of interest to obtain various xanthone derivatives. In this study, a series of twenty-nine new xanthone derivatives (**2**–**30**) with seven types of side chains, alkyl, alkenyl, alkynyl, alkylphenyl, ether, ester, and hydroxyl substituents were synthesised. The chemical structures of the xanthone derivatives were elucidated by spectroscopic analyses, including mass spectrometry (MS), nuclear magnetic resonance (NMR), and Fourier-transform infrared (FTIR). Moreover, crystal structures for compounds **5** and **13** were determined through single-crystal X-ray diffraction analysis to further support the spectroscopy data. The xanthone derivatives were evaluated for their AChE and BChE inhibitory activities by using Ellman's method with minor modification[41]. The enzyme kinetic study of the AChE inhibition by compounds **23** and **28** was reported in this paper. Furthermore, molecular docking of compound **23** was performed in order to elucidate its binding interactions with AChE.

Material and methods

The solvents (analytical grade), silica gel 60, and thin-layer chromatography (TLC) silica gel 60 F254 were obtained commercially from Merck (United States). The chemicals and reagents used in the synthesis reactions were obtained from Sigma Aldrich (Germany) with high purity (>95%). Acetylcholinesterase from *Electrophorus electricus* (500 UN), butyrylcholinesterase from *Equine serum* (1.2 KU), acetylthiocholine iodide, *S*-butyrylthiocholine chloride, and 5,5′-Dithiobis (2-nitro benzoic acid) were obtained from Sigma Aldrich. Tacrine (Purity >98%) was obtained from Cayman Chemical. The melting point of derivatives was determined by Electrothermal 9100 Series Apparatus. Mass spectra of derivatives were acquired from Gas Chromatography-Mass Spectrometry (GCMS) (Agilent J&W) equipped with GC column HP-5MS (30 m × 0.25 mm × 0.25 μm). ^{1}H and ^{13}C NMR spectral data of derivatives were obtained from JEOL JNM-ECX 500 or JNM-ECZ 600 R NMR spectrometers. FTIR spectra of derivatives were recorded on Perkin Elmer Spectrum 100 (Perkin Elmer) equipped with attenuated total reflection (ATR). X-ray analysis was performed using Bruker APEX II DUO CCD diffractometer. Optically active xanthones were analysed using polarimeter Optika POL-1 bench polarimeter. The absorbance of the biological assay was measured with microplate reader BioTek Epoch 2.

Synthesis of xanthones

The synthesis of 3-hydroxyxanthone (**1**) was conducted by mixing the salicylic acid with resorcinol in the presence of Eaton's reagent under reflux. The reaction mixture was poured into ice water, filtered, and subsequently washed with water. The dried powder was subjected to solvent extraction by using ethyl acetate and afforded **1**[42]. Xanthone derivatives (**2**–**30**) were then synthesised by mixing **1** and the corresponding bromide with potassium carbonate in acetone under reflux[43]. The reaction scheme is shown in Figure 1. The reaction mixture was continuously stirred under reflux for hours and monitored by TLC. The reaction mixture was mixed with water upon reaction completion and extracted twice by using chloroform. The organic part was washed successively with hydrochloric acid, sodium carbonate solution, and water. The product was then subjected to purification using column chromatography by eluting a series of solvents (hexane, chloroform, and methanol) with increasing polarity over the silica gel. The chemical structure of pure xanthone derivatives was characterised using MS, NMR and FTIR spectroscopic analyses. Single crystals were obtained for compounds **5** and **13**, thus further analysed by using X-ray diffraction. The optical rotation of xanthone derivatives **7**, **29**, and **30** were measured using a polarimeter.

3-hydroxyxanthone (**1**): M.P. 251–253 °C; *m/z*, $C_{13}H_8O_3$: 212, 184, 155, 128, 102, 92, 77, 63, 51; IR ν_{max} cm^{-1}: 3115, 2884, 1641, 1609, 1586, 1566, 1450, 1226; ^{1}H NMR (600 MHz, DMSO-*d6*): δ_H 10.93 (*s*, 1H, OH-3), 8.10 (*dd*, *J* = 2.1, 8.3 Hz, 1H, H-8), 7.99 (*d*, *J* = 9.0 Hz, 1H, H-1), 7.75 (*td*, *J* = 2.1, 7.6 Hz, 1H, H-6), 7.54 (*d*, *J* = 8.3 Hz, 1H, H-5), 7.38 (deformed *t*, *J* = 7.6, 8.3 Hz, 1H, H-7), 6.86 (*dd*, *J* = 2.1, 9.0 Hz, 1H, H-2), 6.82 (*d*, *J* = 2.1 Hz, 1H, H-4); ^{13}C NMR (150 MHz, DMSO-*d6*): δ_C 175.3 (C-9), 164.6 (C-3), 158.1 (C-4a), 156.1 (C-5a), 135.3 (C-6), 128.5 (C-1), 126.4 (C-8), 124.6 (C-7), 121.7 (C-8a), 118.4 (C-5), 114.7 (C-2), 114.5 (C-9a), 102.7 (C-4).

3-Propoxy-9*H*-xanthen-9-one (**2**): Yield: 92%; White amorphous solid; M.P. 120–122 °C; *m/z*, $C_{16}H_{14}O_3$: 254, 212, 195, 184, 155, 139, 128, 113, 102, 92, 77, 63, 51; IR ν_{max} cm^{-1}: 2874, 1654 1623, 1232; ^{1}H NMR (600 MHz, $CDCl_3$): δ_H 8.20 (*d*, *J* = 8.2 Hz, 1H, H-8), 8.10 (*d*, *J* = 8.2 Hz, 1H, H-1), 7.54 (deformed *t*, *J* = 6.8, 8.2 Hz, 1H, H-6), 7.28 (*d*, *J* = 8.2 Hz, 1H, H-5), 7.23 (deformed *t*, *J* = 6.8, 8.2 Hz, 1H, H-7),

6.78 (*dd*, $J = 2.8$, 8.2 Hz, 1H, H-2), 6.67 (*d*, $J = 2.8$, 1H, H-4), 3.88 (*t*, $J = 6.9$ Hz, 2H, H-1′), 1.77 (*m*, 2H, H-2′), 0.99 (*t*, $J = 6.9$ Hz, 3H, H-3′); ^{13}C NMR (150 MHz, $CDCl_3$): δ_C 176.1 (C-9), 164.6 (C-3), 158.0 (C-4a), 156.1 (C-5a), 134.1 (C-6), 128.0 (C-1), 126.5 (C-8), 123.7 (C-7), 121.9 (C-8a), 117.7 (C-5), 115.5 (C-2), 113.6 (C-9a), 100.6 (C-4), 70.1 (C-1′), 22.4 (C-2′), 10.5 (C-3′).

3-Butoxy-9*H*-xanthen-9-one (**3**): Yield: 84%; White amorphous solid; M.P. 115–117 °C; *m/z*, $C_{17}H_{16}O_3$: 268, 212, 184, 155, 139, 121, 92, 63; IR ν_{max} cm^{-1}: 2874, 1647, 1618, 1239; ^{1}H NMR (600 MHz, $CDCl_3$): δ_H 8.26 (*d*, $J = 8.2$ Hz, 1H, H-8), 8.17 (*d*, $J = 9.6$ Hz, 1H, H-1), 7.62 (deformed *t*, $J = 6.9$, 8.2 Hz, 1H, H-6), 7.37 (*d*, $J = 8.2$ Hz, 1H, H-5), 7.30 (deformed *t*, $J = 6.9$, 8.2 Hz, 1H, H-7), 6.86 (*dd*, $J = 2.7$, 9.6 Hz, 1H, H-2), 6.78 (*d*, $J = 2.7$ Hz, 1H, H-4), 4.01 (*t*, $J = 6.9$ Hz, 2H, H-1′), 1.78 (*m*, 2H, H-2′), 1.49 (*m*, 2H, H-3′), 0.97 (*t*, $J = 6.9$ Hz, 3H, H-4′); ^{13}C NMR (150 MHz, $CDCl_3$): δ_C 176.3 (C-9), 164.7 (C-3), 158.1 (C-4a), 156.2 (C-5a), 134.2 (C-6), 128.2 (C-1), 126.7 (C-8), 123.8 (C-7), 122.0 (C-8a), 117.7 (C-5), 115.6 (C-2), 113.7 (C-9a), 100.6 (C-4), 68.5 (C-1′), 31.1 (C-2′), 19.3 (C-3′), 13.9 (C-4′).

3-Isopropoxy-9*H*-xanthen-9-one (**4**): Yield: 9.1%; White amorphous solid; M.P. 76–78 °C; *m/z*, $C_{16}H_{14}O_3$: 254, 212, 184, 155, 139, 128, 102, 92, 77, 63, 51; IR ν_{max} cm^{-1}: 2923, 1659, 1623, 1280; ^{1}H NMR (600 MHz, $CDCl_3$): δ_H 8.31 (*d*, $J = 8.2$ Hz, 1H, H-8), 8.22 (*d*, $J = 8.2$ Hz, 1H, H-1), 7.67 (deformed *t*, $J = 6.9$, 8.2 Hz, 1H, H-6), 7.43 (*d*, $J = 8.2$ Hz, 1H, H-5), 7.35 (deformed *t*, $J = 6.9$, 8.2 Hz, 1H, H-7), 6.89 (*dd*, $J = 2.7$, 8.2 Hz, 1H, H-2), 6.85 (*d*, $J = 2.7$ Hz, 1H, H-4), 4.68 (*m*, 1H, H-1′), 1.41 (*d*, $J = 6.9$ Hz, 6H, H-2′ and H-3′); ^{13}C NMR (150 MHz, $CDCl_3$): δ_C 176.3 (C-9), 163.7 (C-3), 158.2 (C-4a), 156.3 (C-5a), 134.3 (C-6), 128.4 (C-1), 126.7 (C-8), 123.9 (C-7), 122.1 (C-8a), 117.7 (C-5), 115.6 (C-2), 114.3 (C-9a), 101.6 (C-4), 70.9 (C-1′), 21.9 (C-2′ and C-3′).

3-Isobutoxy-9*H*-xanthen-9-one (**5**): Yield: 29%; White crystalline solid; M.P. 108–110 °C; *m/z*, $C_{17}H_{16}O_3$: 268, 212, 184, 155, 139, 119, 102, 77, 57; IR ν_{max} cm^{-1}: 2899, 1659, 1623, 1280; ^{1}H NMR (500 MHz, $CDCl_3$): δ_H 8.32 (*dd*, $J = 2.3$, 8.0 Hz, 1H, H-8), 8.23 (*d*, $J = 8.0$ Hz, 1H, H-1), 7.68 (*dt*, $J = 2.3$, 6.9, 9.2 Hz, 1H, H-6), 7.44 (*d*, $J = 9.2$ Hz, 1H, H-5), 7.35 (deformed *t*, $J = 6.9$, 8.0 Hz, 1H, H-7), 6.94 (*dd*, $J = 2.3$, 8.0 Hz, 1H, H-2), 6.86 (*d*, $J = 2.3$ Hz, 1H, H-4), 3.84 (*d*, $J = 6.9$ Hz, 2H, H-1′), 2.15 (*m*, 1H, H-2′), 1.06 (*d*, $J = 6.9$ Hz, 6H, H-3′ and H-4′); ^{13}C NMR (125 MHz, $CDCl_3$): δ_C 176.4 (C-9), 164.9 (C-3), 158.2 (C-4a), 156.3 (C-5a), 134.3 (C-6), 128.3 (C-1), 126.8 (C-8), 123.9 (C-7), 122.1 (C-8a), 117.8 (C-5), 115.7 C-2), 113.7 (C-9a), 100.7 (C-4), 75.1 (C-1′), 28.2 (C-2′), 19.3 (C-3′ and C-4′).

3-(Isopentyloxy)-9*H*-xanthen-9-one (**6**): Yield: 82%; White crystalline solid; M.P. 83–85 °C; *m/z*, $C_{18}H_{18}O_3$: 282, 212, 184, 155, 139, 92, 71, 55; IR ν_{max} cm^{-1}: 2958, 1651, 1623, 1256; ^{1}H NMR (500 MHz, $CDCl_3$): δ_H 8.24 (*dd*, $J = 2.3$, 8.0 Hz, 1H, H-8), 8.15 (*d*, $J = 9.2$ Hz, 1H, H-1), 7.58 (*dt*, $J = 2.3$, 6.9, 9.2 Hz, 1H, H-6), 7.33 (*d*, $J = 9.2$ Hz, 1H, H-5), 7.27 (deformed *t*, $J = 6.9$, 8.0 Hz, 1H, H-7), 6.83 (*dd*, $J = 2.3$, 9.2 Hz, 1H, H-2), 6.74 (*d*, $J = 2.3$ Hz, 1H, H-4), 4.01 (*t*, $J = 6.9$ Hz, 2H, H-1′), 1.81 (*m*, 1H, H-3′), 1.68 (*m*, 2H, H-2′), 0.95 (*d*, $J = 6.9$ Hz, 6H, H-4′ and H-5′); ^{13}C NMR (125 MHz, $CDCl_3$): δ_C 176.2 (C-9), 164.7 (C-3), 158.0 (C-4a), 156.2 (C-5a), 134.2 (C-6), 128.1 (C-1), 126.6 (C-8), 123.8 (C-7), 122.0 (C-8a), 117.7 (C-5), 115.6 (C-2), 113.7 (C-9a), 100.6 (C-4), 67.2 (C-1′), 37.7 (C-2′), 25.1 (C-3′), 22.6 (C-4′ and C-5′).

(*S*)-3-(2-Methylbutoxy)-9*H*-xanthen-9-one (**7**): Yield: 32%; White amorphous solid; M.P. 46–48 °C; [α] 25/D + 16.5°, in methanol; *m/z*, $C_{18}H_{18}O_3$: 282, 212, 184, 155, 139, 92, 71, 55; IR ν_{max} cm^{-1}: 2969, 1654, 1616, 1256; ^{1}H NMR (500 MHz, $CDCl_3$): δ_H 8.28 (*d*, $J = 8.0$ Hz, 1H, H-8), 8.20 (*d*, $J = 9.2$ Hz, 1H, H-1), 7.63 (*dt*, $J = 2.3$, 6.9, 9.2 Hz, 1H, H-6), 7.39 (*d*, $J = 9.2$ Hz, 1H, H-5), 7.31 (deformed *t*, $J = 6.9$, 8.0 Hz, 1H, H-7), 6.89 (*dd*, $J = 2.3$, 9.2 Hz, 1H, H-2), 6.81 (*d*, $J = 2.3$ Hz, 1H, H-4), 3.89 (*dd*, $J = 5.7$, 9.2 Hz, 1H, H-1′a), 3.81 (*dd*, $J = 6.9$, 9.2 Hz, 1H, H-1′b), 1.90 (*m*, 1H, H-2′), 1.57 (*m*, 1H, H-3′a), 1.28 (*m*, 1H, H-3′b), 1.03 (*d*, $J = 6.9$ Hz, 3H, H-5′), 0.95 (deformed *t*, $J = 6.9$, 8.0 Hz, 3H, H-4′); ^{13}C NMR (125 MHz, $CDCl_3$): δ_C 176.3 (C-9), 164.9 (C-3), 158.1 (C-4a), 156.3 (C-5a), 134.2 (C-6), 128.2 (C-1), 126.7 (C-8), 123.8 (C-7), 122.0 (C-8a), 117.7 (C-5), 115.6 (C-2), 113.7 (C-9a), 100.7 (C-4), 73.5 (C-1′), 34.6 (C-2′), 26.2 (C-3′), 16.5 (C-5′), 11.4 (C-4′).

3-(2-Ethylbutoxy)-9*H*-xanthen-9-one (**8**): Yield: 50%; Colourless oil; *m/z*, $C_{19}H_{20}O_3$: 296, 212, 184, 155, 139, 119, 102, 85, 55; IR ν_{max} cm^{-1}: 2958, 1659, 1623, 1256; ^{1}H NMR (600 MHz, $CDCl_3$): δ_H 8.26 (*d*, $J = 8.2$ Hz, 1H, H-8), 8.17 (*d*, $J = 8.2$ Hz, 1H, H-1), 7.60 (deformed *t*, $J = 6.9$, 8.2 Hz, 1H, H-6), 7.35 (*d*, $J = 8.2$ Hz, 1H, H-5), 7.28 (deformed *t*, $J = 6.9$, 8.2 Hz, 1H, H-7), 6.87 (*dd*, $J = 2.7$, 8.2 Hz, 1H, H-2), 6.79 (*d*, $J = 2.7$ Hz, 1H, H-4), 3.90 (*d*, $J = 6.9$ Hz, 2H, H-1′), 1.68 (*m*, 1H, H-2′), 1.46 (*m*, 4H, H-3′ and H-5′), 0.92 (*t*, $J = 6.9$, 8.2 Hz, 6H, H-4′ and H-6′); ^{13}C NMR (150 MHz, $CDCl_3$): δ_C 176.2 (C-9), 164.9 (C-3), 158.1 (C-4a), 156.2 (C-5a), 134.2 (C-6), 128.1 (C-1), 126.6 (C-8), 123.8 (C-7), 122.0 (C-8a), 117.7 (C-5), 115.6 (C-2), 113.7 (C-9a), 100.6 (C-4), 70.9 (C-1′), 40.8 (C-2′), 23.4 (C-3′ and C-5′), 11.2 (C-4′ and C-6′).

3-((4-Methylpentyl)oxy)-9*H*-xanthen-9-one (**9**): Yield: 83%; White crystalline solid; M.P. 66–68 °C; *m/z*, $C_{19}H_{20}O_3$: 296, 212, 184, 155, 139, 119, 102, 85, 69; IR ν_{max} cm^{-1}: 2958, 1654, 1623, 1261; ^{1}H NMR (600 MHz, $CDCl_3$): δ_H 8.24 (*d*, $J = 8.2$ Hz, 1H, H-8), 8.14 (*d*, $J = 8.2$ Hz, 1H, H-1), 7.58 (deformed *t*, $J = 6.9$, 8.2 Hz, 1H, H-6), 7.33 (*d*, $J = 8.2$ Hz, 1H, H-5), 7.26 (deformed *t*, $J = 6.9$, 8.2 Hz, 1H, H-7), 6.82 (*dd*, $J = 2.7$, 8.2 Hz, 1H, H-2), 6.72 (*s*, 1H, H-4), 3.94 (*t*, $J = 6.9$ Hz, 2H, H-1′), 1.77 (*m*, 2H, H-2′), 1.58 (*m*, 1H, H-4′), 1.31 (*m*, 2H, H-3′), 0.90 (*d*, $J = 6.9$ Hz, 6H, H-5′ and H-6′); ^{13}C NMR (150 MHz, $CDCl_3$): δ_C 176.1 (C-9), 164.7 (C-3), 158.0 (C-4a), 156.2 (C-5a), 134.2 (C-6), 128.1 (C-1), 126.6 (C-8), 123.8 (C-7), 122.0 (C-8a), 117.7 (C-5), 115.6 (C-2), 113.6 (C-9a), 100.6 (C-4), 69.0 (C-1′), 35.1 (C-3′), 27.9 (C-4′), 27.0 (C-2′), 22.6 (C-5′ and C-6′).

3-(Cyclobutylmethoxy)-9*H*-xanthen-9-one (**10**): Yield: 14%; White amorphous solid; M.P. 95–97 °C; *m/z*, $C_{18}H_{16}O_3$: 280, 212, 184, 155, 127, 107, 92, 69, 53; IR ν_{max} cm^{-1}: 2958, 1659, 1623, 1280; ^{1}H NMR (600 MHz, $CDCl_3$): δ_H 8.31 (*dd*, $J = 1.8$, 7.3 Hz, 1H, H-8), 8.23 (*d*, $J = 8.3$ Hz, 1H, H-1), 7.67 (*dt*, $J = 1.8$, 8.3 Hz, 1H, H-6), 7.43 (*d*, $J = 8.3$ Hz, 1H, H-5), 7.35 (deformed *t*, $J = 7.3$, 8.3 Hz, 1H, H-7), 6.93 (*dd*, $J = 2.8$, 8.3 Hz, 1H, H-2), 6.86 (*d*, $J = 2.8$ Hz, 1H, H-4), 4.04 (*d*, $J = 7.3$ Hz, 2H, H-1′), 2.82 (*m*, 1H, H-2′), 2.17 (*m*, 2H, H-4′), 1.95 (*m*, 4H, H-3′ and H-5′); ^{13}C NMR (150 MHz, $CDCl_3$): δ_C 176.4 (C-9), 164.9 (C-3), 158.2 (C-4a), 156.3 (C-5a), 134.3 (C-6), 128.3 (C-1), 126.7 (C-8), 123.9 (C-7), 122.1 (C-8a), 117.8 (C-5), 115.7 (C-2), 113.8 (C-9a), 100.8 (C-4), 72.7 (C-1′), 34.4 (C-2′), 24.9 (C-3′ and C-5′), 18.6 (C-4′).

3-(2-Cyclohexylethoxy)-9*H*-xanthen-9-one (**11**): Yield: 59%; White crystalline solid; M.P. 134–136 °C; *m/z*, $C_{21}H_{22}O_3$: 322, 239, 212, 184, 155, 139, 111, 95, 69, 53; IR ν_{max} cm^{-1}: 2923, 1652, 1623, 1256; ^{1}H NMR (600 MHz, $CDCl_3$): δ_H 8.28 (*dd*, $J = 2.8$, 8.2 Hz, 1H, H-8), 8.19 (*d*, $J = 8.2$ Hz, 1H, H-1), 7.63 (*dd*, $J = 2.8$, 8.2 Hz, 1H, H-6), 7.38 (*d*, $J = 8.2$ Hz, 1H, H-5), 7.31 (*t*, $J = 8.2$ Hz, 1H, H-7), 6.88 (*dd*, $J = 2.8$, 8.2 Hz, 1H, H-2), 6.80 (*d*, $J = 2.8$ Hz, 1H, H-4), 4.06 (*t*, $J = 6.9$ Hz, 2H, H-1′), 1.70 (*m*, 7H, H-2′, H-4′, H-7′a, H-8′), 1.50 (*m*, 1H, H-3′), 1.20 (*m*, 3H, H-5′ and H-7′b), 0.97 (*m*, 2H, H-6′); ^{13}C NMR (150 MHz, $CDCl_3$): δ_C 176.3 (C-9), 164.7 (C-3), 158.1 (C-4a), 156.2 (C-5a), 134.2 (C-6), 128.2 (C-1), 126.7 (C-8), 123.8 (C-7), 122.0 (C-8a), 117.7 (C-5), 115.6 (C-2), 113.7 (C-9a), 100.7 (C-4), 66.8 (C-1′), 36.4 (C-2′), 34.6 (C-3′), 33.4 (C-4′ and C-8′), 26.6 (C-6′), 26.3 (C-5′ and C-7′).

3-(But-3-en-1-yloxy)-9*H*-xanthen-9-one (**12**): Yield: 46%; White amorphous solid; M.P. 85–87 °C; *m/z*, $C_{17}H_{14}O_3$: 266, 237, 212, 184, 155, 139, 121, 92, 75, 55; IR ν_{max} cm^{-1}: 2948, 1654, 1623, 1258; ^{1}H

NMR (600 MHz, $CDCl_3$): δ_H 8.27 (*dd*, $J = 2.1$, 8.3 Hz, 1H, H-8), 8.18 (*d*, $J = 9.0$ Hz, 1H, H-1), 7.63 (*dt*, $J = 2.1$, 6.9, 8.3 Hz, 1H, H-6), 7.37 (*d*, $J = 8.3$ Hz, 1H, H-5), 7.31 (deformed *t*, $J = 6.9$, 8.3 Hz, 1H, H-7), 6.87 (*dd*, $J = 2.8$, 9.0 Hz, 1H, H-2), 6.79 (*d*, $J = 2.8$ Hz, 1H, H-4), 5.88 (*m*, 1H, H-3′), 5.18 (*dd*, $J = 1.4$, 17.2 Hz, 1H, H-4′a), 5.12 (*dd*, $J = 1.4$, 10.3 Hz, 1H, H-4′b), 4.07 (*t*, $J = 6.9$ Hz, 2H, H-1′), 2.57 (*m*, 2H, H-2′); ^{13}C NMR (150 MHz, $CDCl_3$): δ_C 176.3 (C-9), 164.4 (C-3), 158.0 (C-4a), 156.2 (C-5a), 134.3 (C-6), 133.9 (C-3′), 128.3 (C-1), 126.7 (C-8), 123.9 (C-7), 122.0 (C-8a), 117.7 (C-5), 117.6 (C-4′), 115.8 (C-2), 113.6 (C-9a), 100.8 (C-4), 67.9 (C-1′), 33.4 (C-2′).

3-(Pent-4-en-1-yloxy)-9*H*-xanthen-9-one (**13**): Yield: 88%; White crystalline solid; M.P. 86–88 °C; *m/z*, $C_{18}H_{16}O_3$: 280, 239, 212, 184, 155, 139, 121, 92, 69, 53; IR ν_{max} cm^{-1}: 2958, 1647, 1618, 1258; ^1H NMR (600 MHz, $CDCl_3$): δ_H 8.26 (*d*, $J = 8.2$ Hz, 1H, H-8), 8.17 (*d*, $J = 9.6$ Hz, 1H, H-1), 7.61 (*t*, $J = 6.9$ Hz, 1H, H-6), 7.35 (*d*, $J = 8.2$ Hz, 1H, H-5), 7.29 (deformed *t*, $J = 6.9$, 8.2 Hz, 1H, H-7), 6.85 (*dd*, $J = 2.8$, 9.6 Hz, 1H, H-2), 6.76 (*d*, $J = 2.8$ Hz, 1H, H-4), 5.83 (*m*, 1H, H-4′), 5.03 (*m*, 2H, H-5′), 4.01 (deformed *t*, $J = 5.5$, 6.9 Hz, 2H, H-1′), 2.23 (*m*, 2H, H-3′), 1.90 (*m*, 2H, H-2′); ^{13}C NMR (150 MHz, $CDCl_3$): δ_C 176.2 (C-9), 164.6 (C-3), 158.1 (C-4a), 156.2 (C-5a), 137.5 (C-4′), 134.2 (C-6), 128.2 (C-1), 126.6 (C-8), 123.8 (C-7), 122.0 (C-8a), 117.7 (C-5), 115.7 (C-5′), 115.6 (C-2), 113.6 (C-9a), 100.7 (C-4), 67.9 (C-1′), 30.0 (C-3′), 28.2 (C-2′).

3-(Hex-5-en-1-yloxy)-9*H*-xanthen-9-one (**14**): Yield: 81%; White amorphous solid; M.P. 73–75 °C; *m/z*, $C_{19}H_{18}O_3$: 294, 251, 212, 184, 155, 139, 121, 102, 82, 55; IR ν_{max} cm^{-1}: 2850, 1647, 1623, 1256; ^1H NMR (600 MHz, $CDCl_3$): δ_H 8.26 (*d*, $J = 8.2$ Hz, 1H, H-8), 8.17 (*d*, $J = 8.2$ Hz, 1H, H-1), 7.61 (*m*, 1H, H-6), 7.36 (*d*, $J = 8.2$ Hz, 1H, H-5), 7.29 (deformed *t*, $J = 6.9$, 8.2 Hz, 1H, H-7), 6.85 (*dd*, $J = 2.7$, 8.2 Hz, 1H, H-2), 6.76 (*d*, $J = 2.7$ Hz, 1H, H-4), 5.81 (*m*, 1H, H-5′), 5.00 (*m*, 2H, H-6′), 4.00 (deformed *t*, $J = 5.5$, 6.9 Hz, 2H, H-1′), 2.12 (*m*, 2H, H-4′), 1.81 (*m*, 2H, H-2′), 1.56 (*m*, 2H, H-3′); ^{13}C NMR (150 MHz, $CDCl_3$): δ_C 176.2 (C-9), 164.6 (C-3), 158.1 (C-4a), 156.2 (C-5a), 138.3 (C-5′), 134.2 (C-6), 128.2 (C-1), 126.7 (C-8), 123.8 (C-7), 122.0 (C-8a), 117.7 (C-5), 115.7 (C-2), 115.0 (C-6′), 113.6 (C-9a), 100.6 (C-4), 68.5 (C-1′), 33.4 (C-4′), 28.5 (C-2′), 25.3 (C-3′).

3-((2-Methylallyl)oxy)-9*H*-xanthen-9-one (**15**): Yield: 87%; White amorphous solid; M.P. 121–123 °C; *m/z*, $C_{17}H_{14}O_3$: 266, 251, 225, 197, 181, 165, 139, 115, 92, 77, 55; IR ν_{max} cm^{-1}: 2923, 1654, 1623, 1275; ^1H NMR (600 MHz, $CDCl_3$): δ_H 8.20 (*d*, $J = 8.2$ Hz, 1H, H-8), 8.12 (*d*, $J = 8.2$ Hz, 1H, H-1), 7.54 (deformed *t*, $J = 6.9$, 8.2 Hz, 1H, H-6), 7.28 (*d*, $J = 8.2$ Hz, 1H, H-5), 7.23 (deformed *t*, $J = 6.9$, 8.2 Hz, 1H, H-7), 6.82 (*dd*, $J = 2.7$, 8.2 Hz, 1H, H-2), 6.71 (*d*, $J = 2.7$ Hz, 1H, H-4), 5.06 (*s*, 1H, H-3′a), 4.98 (*s*, 1H, H-3′b), 4.42 (*s*, 2H, H-1′), 1.79 (*s*, 3H, H-4′); ^{13}C NMR (150 MHz, $CDCl_3$): δ_C 176.1 (C-9), 164.1 (C-3), 157.9 (C-4a), 156.1 (C-5a), 139.8 (C-2′), 134.2 (C-6), 128.1 (C-1), 126.6 (C-8), 123.8 (C-7), 121.9 (C-8a), 117.7 (C-5), 115.8 (C-2), 113.7 (C-9a), 113.5 (C-3′), 101.1 (C-4), 72.1 (C-1′), 19.4 (C-4′).

3-((3-Methylbut-2-en-1-yl)oxy)-9*H*-xanthen-9-one (**16**): Yield: 84%; White amorphous solid; M.P. 115–117 °C; *m/z*, $C_{18}H_{16}O_3$: 280, 212, 184, 155, 127, 92, 69, 53; IR ν_{max} cm^{-1}: 2958, 1654, 1625, 1287; ^1H NMR (600 MHz, $CDCl_3$): δ_H 8.25 (*dd*, $J = 2.7$, 8.2 Hz, 1H, H-8), 8.16 (*d*, $J = 8.2$ Hz, 1H, H-1), 7.60 (deformed *t*, $J = 6.9$, 8.2 Hz, 1H, H-6), 7.35 (*d*, $J = 8.2$ Hz, 1H, H-5), 7.28 (deformed *t*, $J = 6.9$, 8.2 Hz, 1H, H-7), 6.86 (*dd*, $J = 2.7$, 8.2 Hz, 1H, H-2), 6.78 (*s*, 1H, H-4), 5.46 (*t*, $J = 6.9$ Hz, 1H, H-2′), 4.55 (*d*, $J = 6.9$ Hz, 2H, H-1′), 1.78 (*s*, 3H, H-4′), 1.74 (*s*, 3H, H-5′); ^{13}C NMR (150 MHz, $CDCl_3$): δ_C 176.2 (C-9), 164.4 (C-3), 158.0 (C-4a), 156.2 (C-5a), 139.3 (C-3′), 134.2 (C-6), 128.2 (C-1), 126.6 (C-8), 123.8 (C-7), 122.0 (C-8a), 118.7 (C-2′), 117.7 (C-5), 115.7 (C-2), 113.8 (C-9a), 100.9 (C-4), 65.5 (C-1′), 25.9 (C-4′), 18.4 (C-5′).

3-((4-Methylpent-3-en-1-yl)oxy)-9*H*-xanthen-9-one (**17**): Yield: 77%; White amorphous solid; M.P. 68–70 °C; *m/z*, $C_{19}H_{18}O_3$: 294, 213, 195, 155, 139, 119, 101, 83, 55; IR ν_{max} cm^{-1}: 2909, 1654, 1625, 1263; ^1H NMR (600 MHz, $CDCl_3$): δ_H 8.21 (*d*, $J = 8.2$ Hz, 1H, H-8), 8.11 (*d*, $J = 9.6$ Hz, 1H, H-1), 7.54 (deformed *t*, $J = 6.9$, 8.2 Hz, 1H, H-6), 7.28 (*d*, $J = 8.2$ Hz, 1H, H-5), 7.23 (deformed *t*, $J = 6.9$, 8.2 Hz, 1H, H-7), 6.79 (*dd*, $J = 2.7$, 9.6 Hz, 1H, H-2), 6.68 (*d*, $J = 2.7$ Hz, 1H, H-4), 5.15 (deformed *t*, $J = 6.9$, 8.2 Hz, 1H, H-3′), 3.91 (*t*, $J = 6.9$ Hz, 2H, H-1′), 2.45 (*dd*, $J = 6.9$, 8.2 Hz, 2H, H-2′), 1.68 (*s*, 3H, H-5′), 1.62 (*s*, 3H, H-6′); ^{13}C NMR (150 MHz, $CDCl_3$): δ_C 176.1 (C-9), 164.5 (C-3), 157.9 (C-4a), 156.1 (C-5a), 134.9 (C-4′), 134.1 (C-6), 128.1 (C-1), 126.5 (C-8), 123.7 (C-7), 121.9 (C-8a), 119.1 (C-3′), 117.7 (C-5), 115.6 (C-2), 113.6 (C-9a), 100.6 (C-4), 68.3 (C-1′), 28.0 (C-2′), 25.8 (C-5′), 18.0 (C-6′).

3-(But-2-yn-1-yloxy)-9*H*-xanthen-9-one (**18**): Yield: 56%; White crystalline solid; M.P. 147–149 °C; *m/z*, $C_{17}H_{12}O_3$: 264, 249, 236, 212, 184, 155, 127, 92, 77, 53; IR ν_{max} cm^{-1}: 2983, 2238, 1654, 1618, 1251; ^1H NMR (600 MHz, $CDCl_3$): δ_H 8.30 (*d*, $J = 8.2$ Hz, 1H, H-8), 8.24 (*d*, $J = 8.2$ Hz, 1H, H-1), 7.68 (deformed *t*, $J = 6.9$, 8.2 Hz, 1H, H-6), 7.44 (*d*, $J = 8.2$ Hz, 1H, H-5), 7.35 (deformed *t*, $J = 6.9$, 8.2 Hz, 1H, H-7), 6.97 (*d*, $J = 8.2$ Hz, 1H, H-2), 6.97 (*s*, 1H, H-4), 4.76 (*s*, 2H, H-1′), 1.87 (*d*, $J = 2.7$ Hz, 3H, H-4′); ^{13}C NMR (150 MHz, $CDCl_3$): δ_C 176.4 (C-9), 163.3 (C-3), 157.9 (C-4a), 156.3 (C-5a), 134.4 (C-6), 128.4 (C-1), 126.8 (C-8), 124.0 (C-7), 122.0 (C-8a), 117.8 (C-5), 116.3 (C-2), 113.7 (C-9a), 101.6 (C-4), 85.0 (C-2′), 73.0 (C-3′), 57.0 (C-1′), 3.8 (C-4′).

3-(Pent-2-yn-1-yloxy)-9*H*-xanthen-9-one (**19**): Yield: 83%; White amorphous solid; M.P. 119–121 °C; *m/z*, $C_{18}H_{14}O_3$: 278, 249, 212, 184, 155, 127, 92, 65; IR ν_{max} cm^{-1}: 2972, 2238, 1654, 1618, 1256; ^1H NMR (600 MHz, $CDCl_3$): δ_H 8.21 (*d*, $J = 8.2$ Hz, 1H, H-8), 8.14 (*d*, $J = 8.2$ Hz, 1H, H-1), 7.57 (*t*, $J = 8.2$ Hz, 1H, H-6), 7.32 (*d*, $J = 8.2$ Hz, 1H, H-5), 7.25 (*t*, $J = 8.2$ Hz, 1H, H-7), 6.87 (*dd*, $J = 2.7$, 8.2 Hz, 1H, H-2), 6.84 (*d*, $J = 2.7$ Hz, 1H, H-4), 4.69 (*t*, $J = 2.7$ Hz, 2H, H-1′), 2.19 (*m*, 2H, H-4′), 1.08 (deformed *t*, $J = 6.9$, 8.2 Hz, 3H, H-5′); ^{13}C NMR (150 MHz, $CDCl_3$): δ_C 176.1 (C-9), 163.2 (C-3), 157.8 (C-4a), 156.2 (C-5a), 134.3 (C-6), 128.2 (C-1), 126.6 (C-8), 123.8 (C-7), 121.9 (C-8a), 117.7 (C-5), 116.1 (C-2), 113.6 (C-9a), 101.5 (C-4), 90.7 (C-3′), 73.2 (C-2′), 57.0 (C-1′), 13.6 (C-5′), 12.5 (C-4′).

3-(But-3-yn-2-yloxy)-9*H*-xanthen-9-one (**20**): Yield: 73%; White amorphous solid; M.P. 170–172 °C; *m/z*, $C_{17}H_{12}O_3$: 264, 249, 207, 165, 139, 89, 63; IR ν_{max} cm^{-1}: 2927, 2112, 1637, 1618, 1251; ^1H NMR (600 MHz, $CDCl_3$): δ_H 8.30 (*d*, $J = 8.2$ Hz, 1H, H-8), 8.24 (*d*, $J = 9.6$ Hz, 1H, H-1), 7.67 (deformed *t*, $J = 6.9$, 8.2 Hz, 1H, H-6), 7.44 (*d*, $J = 8.2$ Hz, 1H, H-5), 7.34 (deformed *t*, $J = 6.9$, 8.2 Hz, 1H, H-7), 7.03 (*d*, $J = 2.7$ Hz, 1H, H-4), 6.99 (*dd*, $J = 2.7$, 9.6 Hz, 1H, H-2), 4.97 (*m*, 1H, H-1′), 2.56 (*d*, $J = 2.7$ Hz, 1H, H-3′), 1.72 (*d*, $J = 6.9$ Hz, 3H, H-4′); ^{13}C NMR (150 MHz, $CDCl_3$): δ_C 176.4 (C-9), 162.7 (C-3), 157.9 (C-4a), 156.3 (C-5a), 134.4 (C-6), 128.3 (C-1), 126.7 (C-8), 124.0 (C-7), 122.0 (C-8a), 117.8 (C-5), 116.3 (C-2), 114.1 (C-9a), 102.3 (C-4), 81.8 (C-2′), 75.0 (C-3′), 64.1 (C-1′), 22.1 (C-4′).

3-(Benzyloxy)-9*H*-xanthen-9-one (**21**): Yield: 61%; White crystalline solid; M.P. 178–180 °C; *m/z*, $C_{20}H_{14}O_3$: 302, 183, 155, 127, 91, 65; IR ν_{max} cm^{-1}: 2958, 1637, 1618, 1251; ^1H NMR (500 MHz, $CDCl_3$): δ_H 8.31 (*d*, $J = 6.9$ Hz, 1H, H-8), 8.25 (*d*, $J = 9.2$ Hz, 1H, H-1), 7.67 (*t*, $J = 6.9$ Hz, 1H, H-6), 7.43 (*q*, $J = 8.0$ Hz, 5H, H-3′, H-4′, H-5′, H-6′, H-7′), 7.35 (*q*, $J = 6.9$ Hz, 2H, H-5 & H-7), 7.00 (*dd*, $J = 2.3$, 9.2 Hz, 1H, H-2), 6.94 (*d*, $J = 2.3$ Hz, 1H, H-4), 5.17 (*s*, 2H, H-1′); ^{13}C NMR (125 MHz, $CDCl_3$): δ_C 176.3 (C-9), 164.2 (C-3), 158.1 (C-4a), 156.3 (C-5a), 135.8 (C-2′), 134.4 (C-6), 128.9 (C-4′ and C-6′), 128.5 (C-1), 128.4 (C-5′), 127.6 (C-3′ and C-7′), 126.7 (C-8), 124.0 (C-7), 122.1 (C-8a), 117.8 (C-5), 116.1 (C-2), 113.9 (C-9a), 101.4 (C-4), 70.6 (C-1′).

3-(3-Phenylpropoxy)-9*H*-xanthen-9-one (**22**): Yield: 94%; White amorphous solid; M.P. 100–102 °C; *m/z*, $C_{22}H_{18}O_3$: 330, 212, 184, 155, 139, 118, 91, 65; IR ν_{max} cm^{-1}: 2958, 1659, 1618, 1282; ^1H

NMR (600 MHz, $CDCl_3$): δ_H 8.29 (*dd*, *J* = 2.7, 8.3 Hz, 1H, H-8), 8.19 (*d*, *J* = 8.2 Hz, 1H, H-1), 7.61 (deformed *t*, *J* = 6.9, 8.2 Hz, 1H, H-6), 7.36 (*d*, *J* = 8.2 Hz, 1H, H-5), 7.30 (deformed *t*, *J* = 6.9, 8.2 Hz, 3H, H-7, H-5′, H-9′), 7.21 (deformed *t*, *J* = 6.9, 8.2 Hz, 3H, H-6′, H-7′, H-8′), 6.87 (*dd*, *J* = 2.7, 8.2 Hz, 1H, H-2), 6.74 (*d*, *J* = 2.7 Hz, 1H, H-4), 3.99 (*t*, *J* = 6.9 Hz, 2H, H-1′), 2.82 (deformed *t*, *J* = 6.9, 8.2 Hz, 2H, H-3′), 2.14 (*m*, 2H, H-2′); ^{13}C NMR (150 MHz, $CDCl_3$): δ_C 176.2 (C-9), 164.6 (C-3), 158.0 (C-4a), 156.2 (C-5a), 141.2 (C-4′), 134.3 (C-6), 128.6 (C-6′ and C-8′), 128.6 (C-5′ and C-9′), 128.2 (C-1), 126.7 (C-7′), 126.2 (C-8), 123.9 (C-7), 122.0 (C-8a), 117.7 (C-5), 115.8 (C-2), 113.6 (C-9a), 100.7 (C-4), 67.6 (C-1′), 32.1 (C-3′), 30.6 (C-2′).

3-(4-Phenylbutoxy)-9*H*-xanthen-9-one (**23**): Yield: 90%; White amorphous solid; M.P. 88–90 °C; *m/z*, $C_{23}H_{20}O_3$: 344, 212, 184, 155, 133, 117, 91, 65; IR ν_{max} cm^{-1}: 2944, 1654, 1623, 1286; ^1H NMR (600 MHz, $CDCl_3$): δ_H 8.29 (*dd*, *J* = 2.7, 8.2 Hz, 1H, H-8), 8.19 (*d*, *J* = 8.2 Hz, 1H, H-1), 7.61 (deformed *t*, *J* = 6.9, 8.2 Hz, 1H, H-6), 7.36 (*d*, *J* = 8.2 Hz, 1H, H-5), 7.30 (deformed *t*, *J* = 6.9, 8.2 Hz, 3H, H-7, H-6′ H-10′), 7.20 (*t*, *J* = 8.2 Hz, 3H, H-7′, H-8′, H-9′), 6.84 (*dd*, *J* = 2.7, 8.2 Hz, 1H, H-2), 6.75 (*d*, *J* = 2.7 Hz, 1H, H-4), 3.99 (deformed *t*, *J* = 5.5, 6.9 Hz, 2H, H-1′), 2.70 (*t*, *J* = 6.9 Hz, 2H, H-4′), 1.83 (*m*, 4H, H-2′, H-3′); ^{13}C NMR (150 MHz, $CDCl_3$): δ_C 176.2 (C-9), 164.6 (C-3), 158.1 (C-4a), 156.2 (C-5a), 142.0 (C-5′), 134.3 (C-6), 128.5 (C-7′ and C-9′), 128.2 (C-6′ and C-10′), 126.7 (C-1), 126.0 (C-8 and C-8′), 123.9 (C-7), 122.0 (C-8a), 117.7 (C-5), 115.7 (C-2), 113.6 (C-9a), 100.7 (C-4), 68.5 (C-1′), 35.6 (C-4′), 28.7 (C-2′), 27.8 (C-3′).

3-(3-Methoxypropoxy)-9*H*-xanthen-9-one (**24**): Yield: 72%; White amorphous solid; M.P. 82–83 °C; *m/z*, $C_{17}H_{16}O_4$: 284, 269, 252, 239, 226, 213, 197, 184, 155, 139, 73; IR ν_{max} cm^{-1}: 2934, 1661, 1563, 1282; ^1H NMR (600 MHz, $CDCl_3$): δ_H 8.29 (*d*, *J* = 8.2 Hz, 1H, H-8), 8.21 (*d*, *J* = 8.2 Hz, 1H, H-1), 7.65 (deformed *t*, *J* = 6.9, 8.2 Hz, 1H, H-6), 7.41 (*d*, *J* = 8.2 Hz, 1H, H-5), 7.33 (deformed *t*, *J* = 6.9, 8.2 Hz, 1H, H-7), 6.90 (*d*, *J* = 8.2 Hz, 1H, H-2), 6.85 (*s*, 1H, H-4), 4.15 (deformed *t*, *J* = 5.5, 6.9 Hz, 2H, H-1′), 3.56 (deformed *t*, *J* = 5.5, 6.9 Hz, 2H, H-3′), 3.35 (*s*, 3H, H-4′), 2.09 (*m*, 2H, H-2′); ^{13}C NMR (150 MHz, $CDCl_3$): δ_C 176.3 (C-9), 164.6 (C-3), 158.1 (C-4a), 156.3 (C-5a), 134.3 (C-6), 128.3 (C-1), 126.7 (C-8), 123.9 (C-7), 122.0 (C-8a), 117.8 (C-5), 115.8 (C-2), 113.6 (C-9a), 100.8 (C-4), 68.9 (C-3′), 65.6 (C-1′), 58.8 (C-4′), 29.5 (C-2′).

3-(2-(Methoxymethoxy)ethoxy)-9*H*-xanthen-9-one (**25**): Yield: 77%; White amorphous solid; M.P. 108–109 °C; *m/z*, $C_{17}H_{16}O_5$: 300, 269, 239, 212, 184, 155, 139, 89, 59; IR ν_{max} cm^{-1}: 2923, 1649, 1618, 1258; ^1H NMR (600 MHz, $CDCl_3$): δ_H 8.21 (*d*, *J* = 8.2 Hz, 1H, H-8), 8.13 (*d*, *J* = 8.2 Hz, 1H, H-1), 7.57 (deformed *t*, *J* = 6.9, 8.2 Hz, 1H, H-6), 7.31 (*d*, *J* = 8.2 Hz, 1H, H-5), 7.25 (deformed *t*, *J* = 6.9, 8.2 Hz, 1H, H-7), 6.85 (*dd*, *J* = 2.7, 8.2 Hz, 1H, H-2), 6.76 (*d*, *J* = 2.7 Hz, 1H, H-4), 4.66 (*s*, 2H, H-3′), 4.16 (deformed *t*, *J* = 4.1, 5.5 Hz, 2H, H-1′), 3.87 (deformed *t*, *J* = 4.1, 5.5 Hz, 2H, H-2′), 3.34 (*s*, 3H, H-4′); ^{13}C NMR (150 MHz, $CDCl_3$): δ_C 176.2 (C-9), 164.2 (C-3), 157.9 (C-4a), 156.2 (C-5a), 134.3 (C-6), 128.2 (C-1), 126.6 (C-8), 123.9 (C-7), 121.9 (C-8a), 117.7 (C-5), 115.9 (C-2), 113.5 (C-9a), 100.8 (C-4), 96.7 (C-3′), 67.9 (C-1′), 65.6 (C-2′), 55.4 (C-4′).

3-(2-(2-Methoxyethoxy)ethoxy)-9*H*-xanthen-9-one (**26**): Yield: 70%; White amorphous solid; M.P. 73–75 °C; *m/z*, $C_{18}H_{18}O_5$: 314, 282, 256, 239, 212, 184, 155, 139, 119, 103, 75, 59; IR ν_{max} cm^{-1}: 2899, 1623, 1469, 1256; ^1H NMR (600 MHz, $CDCl_3$): δ_H 8.17 (*dd*, *J* = 2.7, 8.2 Hz, 1H, H-8), 8.08 (*d*, *J* = 8.2 Hz, 1H, H-1), 7.54 (deformed *t*, *J* = 6.9, 8.2 Hz, 1H, H-6), 7.27 (*d*, *J* = 8.2 Hz, 1H, H-5), 7.22 (deformed *t*, *J* = 6.9, 8.2 Hz, 1H, H-7), 6.81 (*dd*, *J* = 2.7, 8.2 Hz, 1H, H-2), 6.71 (*s*, 1H, H-4), 4.12 (deformed *t*, *J* = 4.1, 5.5 Hz, 2H, H-1′), 3.80 (deformed *t*, *J* = 4.1, 5.5 Hz, 2H, H-2′), 3.64 (deformed *t*, *J* = 4.1, 5.5 Hz, 2H, H-4′), 3.49 (*dd*, *J* = 4.1, 5.5 Hz, 2H, H-3′), 3.30 (*s*, 3H, H-5′); ^{13}C NMR (150 MHz, $CDCl_3$): δ_C 176.1 (C-9), 164.2 (C-3), 157.9 (C-4a), 156.1 (C-5a), 134.2 (C-6), 128.1 (C-1), 126.5 (C-8), 123.8 (C-7), 121.9 (C-8a), 117.7 (C-5), 115.8 (C-2), 113.6 (C-9a), 100.8 (C-4), 72.0 (C-4′), 70.9 (C-1′), 69.4 (C-3′), 68.0 (C-2′), 59.1 (C-5′).

Methyl 2-((9-oxo-9*H*-xanthen-3-yl)oxy)acetate (**27**): Yield: 92%; White amorphous solid; M.P. 151–152 °C; *m/z*, $C_{16}H_{12}O_5$: 284, 225, 195, 155, 139, 119, 92, 63; IR ν_{max} cm^{-1}: 2958, 1623, 1464, 1256; ^1H NMR (600 MHz, $CDCl_3$): δ_H 8.26 (*d*, *J* = 8.2 Hz, 1H, H-8), 8.22 (*d*, *J* = 9.6 Hz, 1H, H-1), 7.65 (*t*, *J* = 6.9 Hz, 1H, H-6), 7.39 (*d*, *J* = 6.9 Hz, 1H, H-5), 7.32 (deformed *t*, *J* = 6.9, 8.2 Hz, 1H, H-7), 6.94 (*dd*, *J* = 2.7, 9.6 Hz, 1H, H-2), 6.81 (*d*, *J* = 2.7 Hz, 1H, H-4), 4.73 (*s*, 2H, H-1′), 3.81 (*s*, 3H, H-3′); ^{13}C NMR (150 MHz, $CDCl_3$): δ_C 176.2 (C-9), 168.5 (C-2′), 163.0 (C-3), 157.8 (C-4a), 156.2 (C-5a), 134.5 (C-6), 128.7 (C-1), 126.7 (C-8), 124.1 (C-7), 121.9 (C-8a), 117.8 (C-5), 116.6 (C-2), 113.2 (C-9a), 101.4 (C-4), 65.3 (C-1′), 52.6 (C-3′).

Ethyl 2-((9-oxo-9*H*-xanthen-3-yl)oxy)acetate (**28**): Yield: 77%; White amorphous solid; M.P. 123–124 °C; *m/z*, $C_{17}H_{14}O_5$: 298, 225, 195, 155, 139, 119, 92, 63; IR ν_{max} cm^{-1}: 2983, 1618, 1464, 1207; ^1H NMR (500 MHz, $CDCl_3$): δ_H 8.28 (*d*, *J* = 8.0 Hz, 1H, H-8), 8.24 (*d*, *J* = 9.2 Hz, 1H, H-1), 7.66 (*m*, 1H, H-6), 7.41 (*d*, *J* = 8.0 Hz, 1H, H-5), 7.33 (*t*, *J* = 8.0 Hz, 1H, H-7), 6.95 (*dd*, *J* = 2.3, 8.0 Hz, 1H, H-2), 6.83 (*d*, *J* = 2.3 Hz, 1H, H-4), 4.72 (*s*, 2H, H-1′), 4.28 (*q*, *J* = 6.9 Hz, 2H, H-3′), 1.30 (*t*, *J* = 6.9 Hz, 3H, H-4′); ^{13}C NMR (125 MHz, $CDCl_3$): δ_C 176.2 (C-9), 168.0 (C-2′), 163.1 (C-3), 157.8 (C-4a), 156.3 (C-5a), 134.5 (C-6), 128.6 (C-1), 126.7 (C-8), 124.0 (C-7), 122.0 (C-8a), 117.8 (C-5), 116.6 (C-2), 113.2 (C-9a), 101.4 (C-4), 65.5 (C-1′), 61.8 (C-3′), 14.2 (C-4′).

(*R*)-3-(3-Hydroxy-2-methylpropoxy)-9*H*-xanthen-9-one (**29**): Yield: 95%; White amorphous solid; M.P. 149–150 °C; [α] 25/D −54.5°, in methanol; *m/z*, $C_{17}H_{16}O_4$: 284, 212, 184, 155, 139, 55; IR ν_{max} cm^{-1}: 3451, 2923, 1618, 1464, 1256; ^1H NMR (600 MHz, $CDCl_3$): δ_H 8.29 (*d*, *J* = 8.2 Hz, 1H, H-8), 8.17 (*d*, *J* = 8.2 Hz, 1H, H-1), 7.66 (*m*, 1H, H-6), 7.40 (*d*, *J* = 8.2 Hz, 1H, H-5), 7.34 (deformed *t*, *J* = 6.9, 8.2 Hz, 1H, H-7), 6.88 (*dd*, *J* = 2.7, 8.2 Hz, 1H, H-2), 6.82 (*d*, *J* = 2.7 Hz, 1H, H-4), 4.04 (*m*, 2H, H-1′), 3.73 (*m*, 1H, H-3′), 2.23 (*m*, 2H, H-2′), 1.08 (*d*, *J* = 6.9 Hz, 3H, H-4′); ^{13}C NMR (150 MHz, $CDCl_3$): δ_C 176.4 (C-9), 164.6 (C-3), 158.0 (C-4a), 156.3 (C-5a), 134.4 (C-6), 128.3 (C-1), 126.7 (C-8), 123.9 (C-7), 122.0 (C-8a), 117.8 (C-5), 115.8 (C-2), 113.6 (C-9a), 100.8 (C-4), 70.9 (C-1′), 65.0 (C-3′), 35.7 (C-2′), 13.7 (C-4′).

(*S*)-3-(3-hydroxy-2-methylpropoxy)-9*H*-xanthen-9-one (**30**): Yield: 58%; White amorphous solid; M.P. 149–151 °C; [α] 25/D + 17.7°, in methanol; *m/z*, $C_{17}H_{16}O_4$: 284, 212, 184, 139, 92, 55; IR ν_{max} cm^{-1}: 3448, 2923, 1618, 1466, 1258; ^1H NMR (600 MHz, $CDCl_3$): δ_H 8.29 (*d*, *J* = 8.2 Hz, 1H, H-8), 8.17 (*d*, *J* = 9.6 Hz, 1H, H-1), 7.66 (*m*, 1H, H-6), 7.40 (*d*, *J* = 8.2 Hz, 1H, H-5), 7.34 (deformed *t*, *J* = 6.9, 8.2 Hz, 1H, H-7), 6.88 (*dd*, *J* = 2.7, 9.6 Hz, 1H, H-2), 6.82 (*d*, *J* = 2.7 Hz, 1H, H-4), 4.04 (*m*, 2H, H-1′), 3.73 (*m*, 2H, H-3′), 2.23 (*m*, 1H, H-2′),1.08 (*d*, *J* = 6.9 Hz, 3H, H-4′); ^{13}C NMR (150 MHz, $CDCl_3$): δ_C 176.4 (C-9), 164.6 (C-3), 158.1 (C-4a), 156.3 (C-5a), 134.4 (C-6), 128.3 (C-1), 126.7 (C-8), 123.9 (C-7), 122.0 (C-8a), 117.8 (C-5), 115.8 (C-2), 113.6 (C-9a), 100.8 (C-4), 71.0 (C-1′), 65.1 (C-3′), 35.7 (C-2′), 13.7 (C-4′).

X-ray diffraction analysis

X-ray analyses for compounds **5** and **13**, which exist in the single crystal form, were performed using Bruker APEX II DUO CCD diffractometer, employing MoKα radiation (λ = 0.71073 Å) with φ and ω scans, at room temperature. Data reduction and absorption correction were performed using the SAINT and SADABS programs[44]. Both structures were solved by direct methods and refined by full-matrix, least-squares techniques on F^2 using the SHELXTL software package[45,46]. All H atoms were placed in geometrically idealised positions and constrained to ride on their parent atoms with

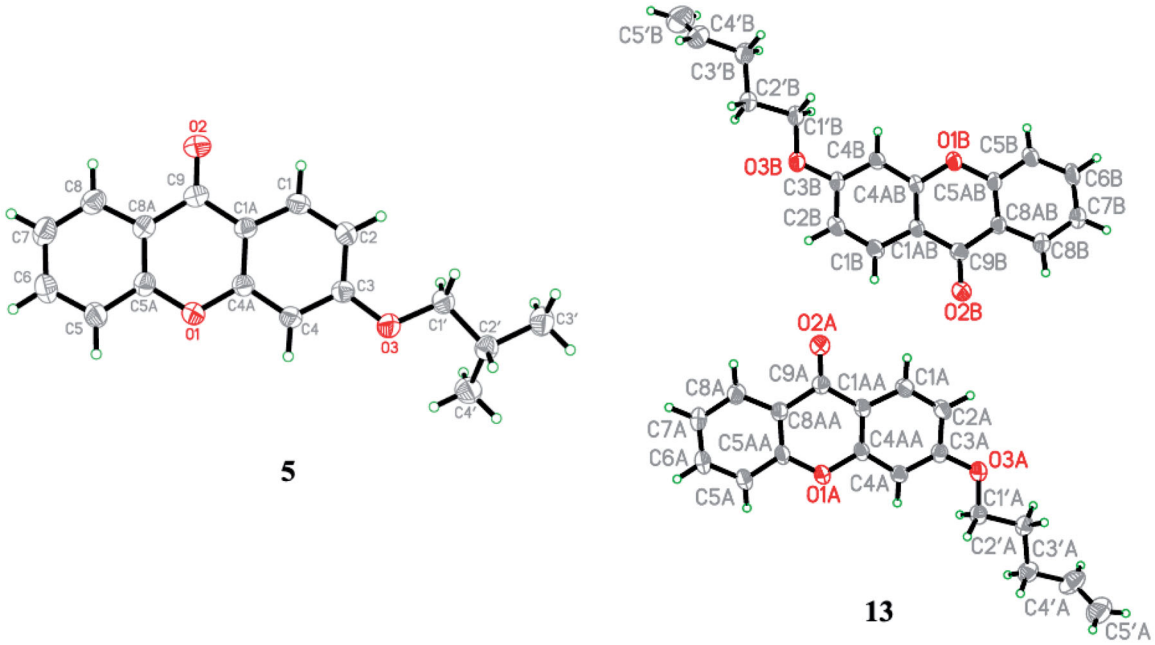

Figure 2. ORTEP diagram of compounds **5** and **13**.

Table 1. Crystal data and parameters for the structure refinement of **5** and **13**.

Compound	5	13
CCDC number	1863942	1863946
Molecular formula	$C_{17}H_{16}O_3$	$C_{18}H_{16}O_3$
Molecular weight	268.30	280.31
Crystal system	Monoclinic	Triclinic
Space group	$P2_1/c$	$P\bar{1}$
a (Å)	12.1571 (13)	7.503 (6)
b (Å)	5.0697 (5)	11.297 (9)
c (Å)	21.793 (2)	17.769 (14)
α (°)	90	98.931 (10)
β (°)	98.156 (5)	95.355 (11)
γ (°)	90	103.272 (10)
V (Å^3)	1329.6 (2)	1435 (2)
Z	4	4
Dcalc (Mg m^{-3})	1.340	1.297
Crystal dimensions (mm)	0.49 × 0.08 × 0.06	0.38 × 0.27 × 0.25
μ (mm^{-1})	0.09	0.09
T_{min}/T_{max}	0.747, 0.977	0.658, 0.952
Reflections measured	32949	18566
Ranges/indices (h, k, l)	−14→14, −6→6, −25→25	−8→8, −13→13, −21→21
θ limit (°)	2.4–29.8	2.4–21.9
Unique reflections	2325	5042
Observed reflections ($I > 2\sigma(I)$)	1334	2531
Parameters	181	379
Goodness of fit on F^2	1.03	1.08
R_1, wR_2 [$I \geq 2\sigma(I)$]	0.066, 0.172	0.096, 0.266
R_1, wR_2 [all data]	0.120, 0.216	0.165, 0.335

C–H distance in the range of 0.93–0.97 Å and $U_{iso}(H) = 1.2\,U_{eq}(C)$, while $U_{iso}(H)$ for methyl H atoms were set at $1.5\,U_{eq}(C)$ and each group was allowed to rotate freely about its C–C bond. Crystallographic data for compounds **5** and **13** had been deposited at the Cambridge Crystallographic Data Centre (CCDC) with the deposition numbers of 1863942 and 1863946, respectively. Copies of available material can be obtained free of charge on application to the CCDC, 12 Union Road, Cambridge CB2 1EZ, UK, (Fax: +44-(0)1223–336033 or e-mail: deposit@ccdc.cam.ac.uk). The ORTEP (Oak Ride Thermal Ellipsoid Plot Program) of **5** and **13** are shown in Figure 2 and X-ray crystallographic data are presented in Table 1.

Biological assay

Cholinesterase inhibition activity assay

The assay was carried out according to Ellman's method with slight modification by using AChE and BChE[41]. Tacrine was used as a positive control in this assay. Acetylcholinesterase (AChE) (source: *Electrophorus electricus*), butyrylcholinesterase (BChE) (source: Equine serum), acetylthiocholine iodide (ATCI), *S*-butyrylthiocholine chloride (BTCC) and 5,5′-dithiobis (2-nitrobenzoic acid) (DTNB) were dissolved in sodium phosphate buffer (100 mM, pH 8.0). A stock solution of tacrine and samples were prepared in DMSO and further diluted using sodium phosphate buffer. Firstly, the samples were evaluated at the concentration of 1 and 4 μg/mL for AChE and BChE inhibition activities, respectively. The xanthone derivatives that showed more than 50% of enzyme inhibition were further evaluated in a series of concentration from 0.0625 to 1 μg/mL to determine their IC_{50} values. Briefly, 200 μL of DTNB (0.5 mg/mL) was added into a 96 well plate for AChE assay while 150 μL of sodium phosphate buffer and 50 μL of DTNB (0.5 mg/mL) were added for BChE assay. Then, 20 μL of the compounds were added into the wells together with 20 μL of AChE solution (0.266 U/mL) or BChE solution (0.15 U/mL). The mixtures were incubated for 15 min in the dark at 37 °C. After that, 10 μL of ATCI (0.2052 mg/mL) or BTCC (0.5 mg/mL) were added into the wells to initiate the reaction. Immediately, the absorbance was measured at 412 nm for 10 times with 1-min interval. The percentage of enzyme inhibition was calculated using the following formula:

$$\text{Percentage inhibition} = \left(\text{Slope}_{\text{control}} - \text{Slope}_{\text{drug}} / \text{Slope}_{\text{control}}\right) \times 100$$

AChE enzyme kinetic study

The enzyme inhibition modes of AChE by compounds **23** and **28** were evaluated by using the substrate ATCI in the range of concentrations (0.43, 0.86, 1.73, 3.45, and 6.90 mM) with the absence and presence of compounds. The concentration of the compound used were 2.91, 0.73, 0.36 and 0.18 μM for **23** and 3.36, 1.68, 0.84 and 0.42 μM for **28**. The mode of inhibition was determined by using Lineweaver–Burk plot[47].

Computational studies

Flexible docking

The X-ray crystal structure of *Electrophorus electricus* acetylcholinesterase (PDB ID: 1C2O) was retrieved from the protein database bank (PDB) (http://www.rcsb.org). Although the resolution is 4.2 Å, visual inspection showed minimal difference in the position of the amino acid residues in the active site as compared with some high-resolution crystal structures available in the PDB. Thus, this protein crystal structure was deemed suitable to be used in our docking study. The ligand-binding site was identified based on the position of the inhibitor-binding site as reported by literature. Residues W108, E224, S225, Y313, Y355, F356 and Y359 were specifically selected as flexible based on the observation by[48], in which they superposed 68 AChE complex crystal structures over the crystal structure of human apo-AChE (PDB ID: 4PQE)[48]. Additionally, several conserved water molecules (structural water molecules) were inserted manually to the binding site according to the protein crystal structure (PDB ID: 1ACJ) to create a more realistic environment of AChE binding site[49].

Both compound **23** and tacrine were then prepared and minimised before the docking procedure. The DS Flexible Docking module was adopted for the receptor-ligand docking. The ligand was docked to the active site of each receptor conformation using LibDock. The maximum number of compounds conformations generated were set at 225 numbers followed by clustering to remove similar ligand pose. The selected protein side-chains were refined in the presence of the rigid ligand using ChiRotor and the final ligand pose was optimised using CDOCKER.

Statistical analysis

The values were expressed as mean ± SD from three independent experiments. The statistical significance was calculated by one-way analysis of variance (ANOVA), followed by Tukey's test. The percentage inhibition of AChE and BChEand Lineweaver-Burk plot were plotted using GraphPad Prism version 7.

Results and discussion

Characterisation of 3-hydroxyxanthone (1)

The structure of 3-hydroxyxanthone (**1**) was elucidated using MS, FTIR and NMR spectroscopies. The mass spectrum demonstrated a molecular ion peak at *m/z* 212, which corresponds to the molecular weight of **1**. The FTIR spectrum displayed absorptions of free –OH at 3112 cm^{-1}, sp^3 C–H at 2888 cm^{-1}, C=O at 1644 cm^{-1}, aromatic C=C at 1607 cm^{-1}, and C–O at 1228 cm^{-1}. The ^{1}H NMR spectrum showed the presence of a chelated hydroxyl group at position C-3, as indicated by a singlet peak at the downfield region, δ 10.93. The de-shielding effects of carbon nucleus by oxygen atom leads to the exposure of the higher external magnetic field, which in turn, requires higher frequency to achieve resonance and results in a peak in a downfield region. Besides, three doublets were detected at δ 7.99, 7.54, and 6.82 for H-1, H-5, and H-4, respectively, while a deformed triplet peak was spotted at δ 7.38 for H-7. Two sets of doublet of doublet were observed at δ 8.10 and 6.86 with respect to H-8 and H-2, while a triplet of doublet was detected at δ 7.75 for H-6. These signals revealed the presence of two aromatic rings in the main skeleton of xanthone. For ^{13}C NMR, the highest chemical shift was given by the carbonyl carbon at C-9 (δ 175.3) and followed by the hydroxyl carbon at C-3 (δ 164.6). These peaks were attributed to the electron-withdrawing effect of oxygen atom. On the other hand, the aromatic carbon signals of xanthone skeleton were found in the range of δ 103 to 158 ppm. The ^{1}H and ^{13}C NMR spectral data and melting point of **1** are in good agreement with the literature data[50,51] and were used as the standard spectra for the spectral data analyses of xanthone derivatives (**2–30**).

Characterisation of xanthone derivatives (2–30)

The mass spectra of the xanthone derivatives demonstrated molecular ion peaks that correspond to the molecular weight of the respective compounds. The ^{1}H NMR spectral data of the xanthone derivatives (**2–30**) revealed an absence of the chelated hydroxyl singlet peak at the chemical shift region near δ 11 ppm. Moreover, ^{1}H NMR spectra of the xanthone derivatives showed additional peaks when compared to that of **1**. For xanthone derivatives **2**–**20**, **24**–**30**, additional peaks appeared in different regions of chemical shifts from those represented the main skeleton (δ 6.8–8.3), which was seen in the spectrum of **1**. Xanthone derivatives **21**–**23**, which bear a phenyl substituent have additional peaks in their ^{1}H NMR spectra that are overlapped with the chemical shift region of the main skeleton of xanthone (**1**). Analyses of these additional peaks were found to be consistent with the proposed structures. Based on the integration values in the spectra, the number of protons are in agreement with that in the structures.

Similarly, additional peaks were observed in the ^{13}C NMR spectra for the xanthone derivatives (**2–30**). Besides, the absence of a broad hydroxyl (–OH) peak at the region of 3100–3500 cm^{-1} in the FTIR spectra of xanthone derivatives **2**–**28** further confirmed the successful attachment of the substituent groups at C-3 position of **1**. The results showed that the hydroxyl group at position C-3 was successfully substituted by the respective hydrocarbon, ether, ester, and hydroxyl substituent groups.

AChE and BChE inhibitory activities

The parent compound, 3-hydroxyxanthone, **1**, together with its derivatives **2–30** were evaluated for their cholinesterase inhibitory activities using the Ellman's method with minor modifications. Tacrine was used as a positive control throughout the experiment. To begin with, compounds **1**–**30** were evaluated with AChE and BChE inhibition activities at the concentration of 1 μg/mL. Remarkably, all compounds exhibited good to moderate inhibition activity against AChE but not BChE. The results strongly indicate that the compounds were more selective towards AChE over BChE. A previous molecular docking study focussed on 3,5-dimethoxy-*N*-methylenebenzenamine derivatives showed that a small compound is unable to bind efficiently to the BChE binding site which has a larger volume of the bottom gorge. Thus, BChE binding site is ideal in accommodating bulkier substrate. As a result, all the derivatives with small substituent groups such as methoxy, hydroxy, and nitro groups, showed potent AChE inhibition effect and highly selective towards AChE over BChE[52]. Moreover, a recent study reported an oxygenated xanthone with bulky substituents of geranyl unit at C-8 and acetate at C-14 as a potent and selective BChE inhibitor. Besides two hydrogen bonding between the xanthone core and Tyr128 and Asn68 from BChE active pocket, hydrophobic interactions were observed between the geranyl and Trp82 from the choline-binding site, and His438 and Trp430 from the catalytic active site[53], deducing that a more bulky substituent is needed for BChE inhibitory effect. The synthesised xanthone derivatives in this study are considered as

Table 2. AChE and BChE inhibitory activities of compounds **1**–**30**.

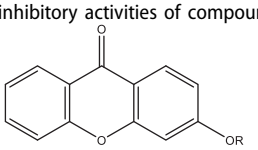

Compound	Substituent, *R* group	AChE IC_{50} (μM)	BChE Percentage of inhibition at 4 μg/mL (%)
1	H	2.39 ± 0.11^{a}	6.55 ± 0.82
2	Propyl	1.86 ± 0.04^{bcd}	11.94 ± 1.74
3	Butyl	1.40 ± 0.14^{efgh}	17.58 ± 1.89
4	Isopropyl	1.41 ± 0.13^{efgh}	20.68 ± 1.75
5	Isobutyl	1.18 ± 0.11^{ghij}	9.78 ± 1.22
6	Isopentyl	1.84 ± 0.21^{bcd}	5.47 ± 0.61
7	(*S*)-2-Methylbutyl	1.74 ± 0.20^{cde}	24.78 ± 1.96
8	2-Ethylbutyl	1.15 ± 0.19^{hij}	12.62 ± 1.26
9	2-Methylpentyl	2.07 ± 0.06^{abc}	11.76 ± 0.98
10	Methylcyclobutyl	1.61 ± 0.11^{def}	7.01 ± 1.16
11	Ethylcyclohexyl	1.27 ± 0.13^{fghij}	24.33 ± 2.29
12	Buten-3-yl	2.09 ± 0.21^{abc}	5.33 ± 0.17
13	Penten-4-yl	>3.57	20.89 ± 3.07
14	Hexen-5-yl	>3.40	16.35 ± 1.34
15	2-Methylpropenyl	1.60 ± 0.15^{defg}	2.33 ± 0.30
16	2-Methylbuten-2-yl	1.86 ± 0.15^{bcd}	7.96 ± 1.22
17	2-Methylpenten-2-yl	1.06 ± 0.12^{hij}	20.94 ± 3.03
18	2-Butynyl	>3.79	4.53 ± 0.88
19	2-Pentynyl	1.21 ± 0.05^{fghij}	5.24 ± 0.25
20	3-Methyl-propynyl	2.24 ± 0.17^{ab}	5.00 ± 0.74
21	Benzyl	0.99 ± 0.19^{hij}	5.04 ± 0.70
22	Phenylpropyl	1.22 ± 0.12^{fghij}	15.50 ± 1.93
23	Phenylbutyl	0.88 ± 0.04^{j}	9.19 ± 0.55
24	Methoxypropyl	>3.52	11.00 ± 1.38
25	Methoxymethoxyethyl	1.37 ± 0.12^{efghi}	10.26 ± 1.24
26	Methoxyethoxyethyl	0.97 ± 0.06^{ij}	17.76 ± 1.60
27	Methyl acetate	1.28 ± 0.13^{fghij}	7.69 ± 0.34
28	Ethyl acetate	0.88 ± 0.15^{j}	4.11 ± 0.35
29	(*R*)-Hydroxyl-2-methylpropyl	>3.52	13.94 ± 0.96
30	(*S*)-Hydroxyl-2-methylpropyl	>3.52	5.48 ± 0.31
Tacrine		0.06 ± 0.00^{k}	96.55 ± 0.18*

Data represents the mean ± SD of three independent experiments; Different letters indicated significantly different at $p < 0.05$ between sample groups among AChE assay.
*The concentration of tacrine (positive control) used in the experiment was 1 μg/mL.

smaller compounds and thus exhibiting lower inhibitory effect towards BChE, if compared to AChE.

Overall, most of the compounds are able to reduce 50% of AChE activity at the concentration of 1 μg/mL, except for **13**, **14**, **18**, **24**, **29**, and **30**. The active compounds were then determined for their IC_{50} values and the result was tabulated in Table 2. Compounds **23** and **28** are the most potent xanthone derivatives with the same IC_{50} values of 0.88 μM. Conversely, the xanthone derivatives exhibited weak BChE inhibition even a higher concentration of 4 μg/mL. Thus, the IC_{50} values were not determined for BChE inhibition activities (Figures S1 and S2).

The result showed that twenty-three synthesised xanthones exhibited significant AChE inhibition with low IC_{50} values ranging from 0.88 to 2.39 μM although their activities are weaker than the positive control, tacrine. The results are in good agreement with previous studies that xanthones are potential AChE inhibitors. By comparing their structural features, the reported xanthones are also bearing different substituents, particularly methoxyl, prenyl, benzyl, pyranyl, or hydroxyl, which were attached at different positions on the xanthone main skeleton[15,32,54–57].

Overall, all the xanthone derivatives exhibited stronger AChE inhibitory effect than the parent compound (**1**) except for **9**, **12**, and **20** that exhibited comparable effects with **1**. The results are consistent with a previous study that etherified xanthones with alkyl groups, particularly methoxyl, prenylated oxyl, and allyl oxyl group at the position 3, possessed stronger anti-AChE activity than those with a hydroxyl group[58]. SAR analysis revealed that hydrophobic interaction at position 3 of xanthone contributes positive effects to the AChE inhibition. By comparing the substituent groups attached to the C-3 position of the xanthone, the derivatives (**24**–**28**) with ether (ROR′) and ester (RCOOR′) groups demonstrated good AChE inhibition activities (except **24**). The results indicated that the hydrogen bonding, contributed by –C–O–C from the substituent groups, play a vital role in the inhibitory activities, in addition to the hydrophobic interactions. The finding is supported by a previous molecular docking study where potent AChE inhibition effects of three xanthones, namely α-mangostin, γ-mangostin, and garcinone C were suggested to be contributed by the strong hydrogen bonding and π–σ interaction with several critical amino acid residues in the active sites of AChE[15]. Hydrogen bond was formed in between hydroxylated prenyl group at C-8 of garcinone C and His 440 of the AChE catalytic site. A π–σ interaction, on the other hand, formed between hydroxyl group at C-6 of garcinone C and Trp 84 from the choline binding site. Likewise, Trp 84 at the choline-binding site forms favourable π–π interactions with xanthone skeleton of α-mangostin and γ-mangostin[15]. Furthermore, another study reported that two oxygen atom at position 5 and 6 from macluraxanthone binds tightly to AChE through hydrogen bondings with the OH of Tyr 124 and O of Tyr 72, as well as hydrophobic interactions between hydrocarbons of macluraxanthone with several subsites, including PAS, anionic subsite (AS) and acyl-binding pocket (ABP) of AChE[55].

The results obtained from the AChE inhibition of xanthone derivatives showed that the chain length of hydrocarbons present in the C-3 side chain of xanthone influences the level of activities. Compound **3**, which bears a 4-carbons chain, exhibited stronger inhibition activity if compared to **2** (3-carbons chain). A similar trend was observed for compounds **12–14** that bear an unsaturated 4- to 6-carbons chain. Compound **12** that has a butenyl substituent group showed an enhanced AChE inhibition activity than compounds **13** and **14**. Among the linear type of substituents, our results suggest that a 4-carbons chain length is favourable to AChE inhibition effect either with or without the unsaturated bond. A previous study focussed on the amine side chains of the xanthone reported that elongation of the hydrocarbon chain attached to the xanthone skeleton units resulted in a drastic drop of AChE inhibition activities. The authors reported that three methylene units as the linker carbon between the xanthone skeleton and the amino side chain exhibited the most potent inhibition effect with an IC_{50} value of 2.68 μM[59], which is consistent with our study where compounds **3** and **12** that bear a three methylene unit possessed strong effect with IC_{50} values of 1.40 and 2.09 μM, respectively.

By comparing linear substituent groups of xanthone derivatives with the same carbon chain, the AChE inhibition effects were observed to have an increasing trend from alkynyl, alkenyl to alkyl substituents. The evidence is that the lowest IC_{50} values were found to be exhibited by **3** (butyl), followed by **12** (butenyl) and **18** (butynyl). This might be due to the structural flexibility of **3** that bind sterically to AChE as the inhibition activity are correlated with hydrophobicity, electronic, inductive, or polar properties, and steric effects[60]. However, the introduction of an unsaturated bond into the substituent groups that made up of branched hydrocarbon chain has a different influence on activity, depending on the length of the carbon chain. Xanthone derivative **17** (IC_{50} =

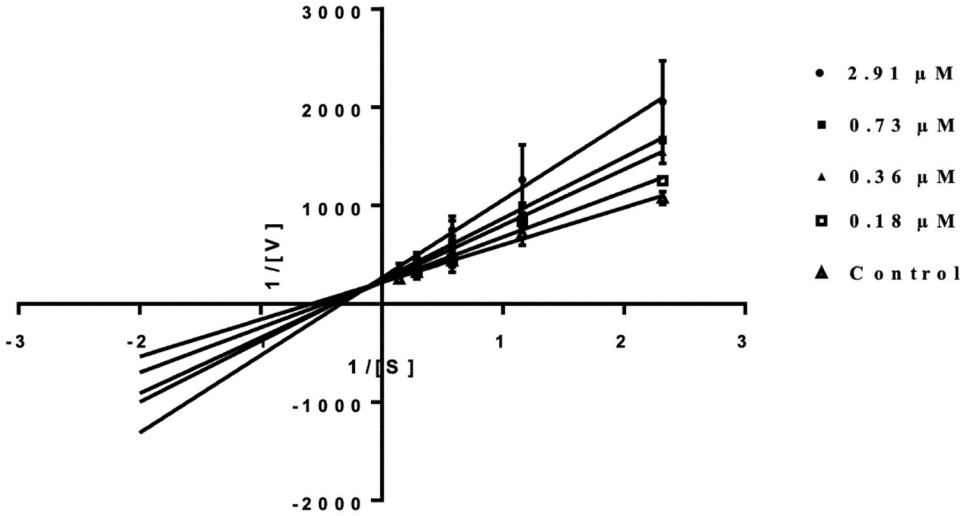

Figure 3. Lineweaver–Burk plot of 3-(4-phenylbutoxy)-9*H*-xanthen-9-one (**23**) against AChE. Bar indicates the standard deviation.

1.06 μM), which has a substituent group of 5-carbons in chain length with an unsaturated bond (2-methylpenten-2-yl) possessed 2-folds stronger inhibitory activities than **9** (IC_{50} = 2.07 μM) that bears a substituent group with the same chain length but without any unsaturated bond (2-methylpentyl). There is no significant difference in AChE inhibition being observed for **5** (isobutyl; IC_{50} = 1.18 μM) and **15** (2-methylpropenyl; IC_{50} = 1.60 μM) and between **6** (isopentyl; IC_{50} = 1.84 μM) and **16** (isopentenyl; IC_{50} = 1.86 μM). Moreover, compound **20** (IC_{50} = 2.24 μM) that consisted of a branched substituent with 3-carbons chain length and a triple bond experienced a drop in activity when compared to compound **5**. Therefore, we anticipated that the xanthone derivatives with branched substituents, the presence of unsaturated bond would improve the AChE inhibition activity for those substituent groups consisting of more than 5-carbons chain length. The finding is further supported by the xanthone derivatives with phenyl substituent, including compounds **21**–**23** that showed good inhibitory effects with IC_{50} values ranging from 0.88 to 1.22 μM. The inhibition potency of phenyl substituted xanthone derivatives could be explained by potential hydrophobic interaction and π–π stacking with the aromatic residues of the enzyme gorge in AChE[61]. A high degree of lipid solubility compound favours the crossing of the blood–brain barrier (BBB) by transmembrane diffusion and also the uptake by the peripheral tissues[62]. Hence, small molecule drugs with molecular weight less than 400 Da and lipid solubility such as the xanthone derivatives synthesised and presented in this study, could potentially cross the BBB and preferred in the drug development for brain diseases[63]. As a summary, eleven xanthone derivatives (**5**, **8**, **11**, **17**, **19**, **21–23**, **26–28**) possessed potent AChE inhibition activity. The overall results deduced that 3-*O*-substituted xanthones that carry a saturated linear hydrocarbon side chain of 4-carbons in chain length with an addition of phenyl group, or diether or ester are beneficial in AChE inhibition activity.

AChE enzyme kinetic analysis

The enzyme inhibition mode of two promising compounds, **23** and **28** against AChE was analysed by a double-reciprocal Lineweaver–Burk plot as shown in Figures 3 and 4. Both the maximal velocity of the AChE enzyme-substrate compound reaction (V_{max}) and the affinity (K_m) were affected by the compound concentration as shown in the kinetic parameters calculated from the double reciprocal trend lines, hence indicating a mixed-mode inhibition. The Michaelis–Menten parameters are tabulated in Table S1. In a mixed-mode inhibition, the inhibitors can bind to the free enzyme or the enzyme-substrate complex. The binding of inhibitors to the enzyme-substrate complex resulted in a reduction in the complex affinity towards substrates, thus explaining the increase in K_m.

Binding interactions of 3-(4-phenylbutoxy)-9H-xanthen-9-one (23) with AChE

It is known that the amino acid residues surrounding the active site of *Electrophorus electricus* AChE are highly identical to the human AChE[64,65]. In general, the active sites of AChE contain anionic catalytic sites which are located at the bottom of the gorge while peripheral anionic binding sites at the entrance (mouth) of the gorge. Inhibitors such as tacrine which is comprised of a small volume group could enter easily into the gorge and interact with the residing active catalytic site Trp86 and Tyr337 residues, which is located at the bottom of the gorge, as observed in the crystal structure and molecular docking study[49]. Similarly, we observed that the xanthone ring could protrude deeply into the active site and interact via extensive π–π stacking with the indole and phenol side chains of Trp86 and Tyr337 (Figure 5). Apart from that, the planar geometry form of the xanthone ring as supported by the XRD analysis could also prove to be an important factor in aiding the compound's binding process. Besides, the position of the carbonyl group of compound **23** is also similar to the amino group of tacrine, which is directed towards the hydration site comprised of D74, T83, W86, N87, and S125 residues. Since these water molecules are highly buried, they could possibly involve in a complex hydrogen bonding interaction with the inhibitors. It is likely that the carbonyl group could form hydrogen-bonding interactions with these buried water molecules thus enforcing its binding in the active site. In addition, the substituted alkyl benzene ring could interact with the phenol side chain of Y72 via π–π interaction further strengthening its binding interactions in the AChE active-site gorge.

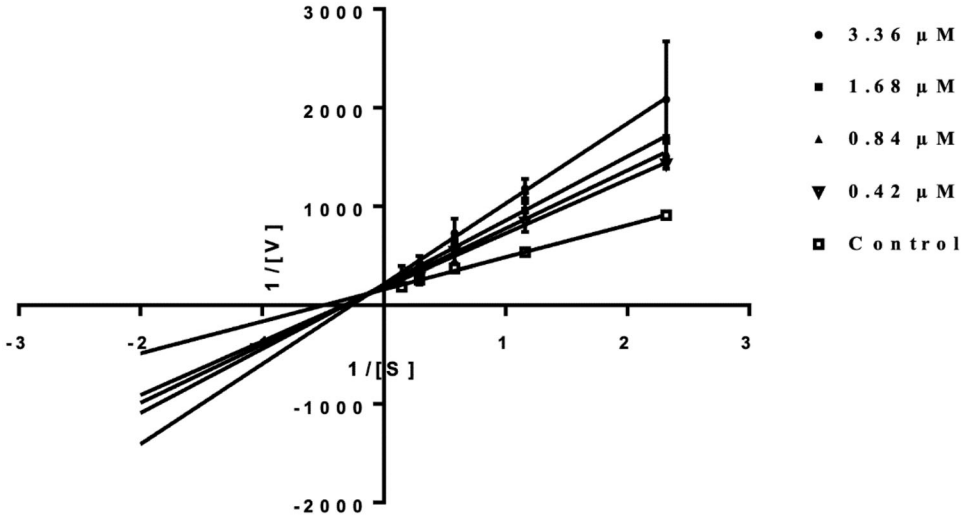

Figure 4. Lineweaver–Burk plot of ethyl 2-((9-oxo-9*H*-xanthen-3-yl)oxy)acetate (**28**) against AChE. Bar indicates the standard deviation.

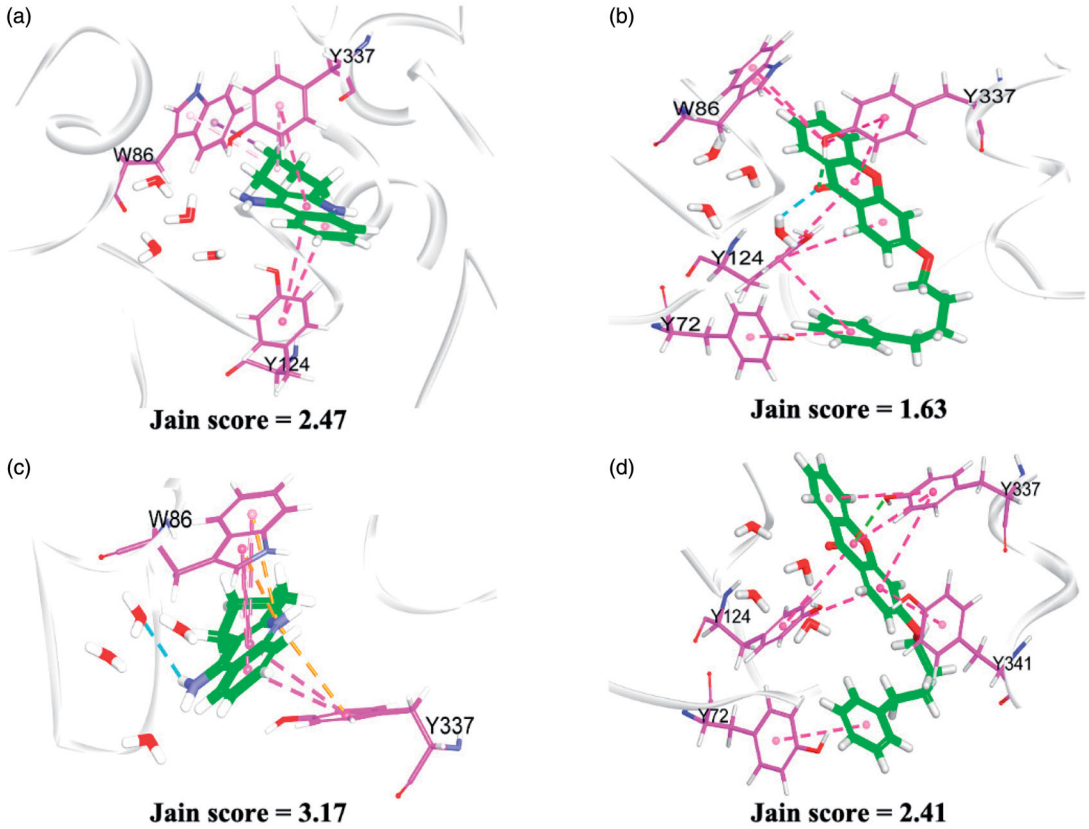

Figure 5. Binding interactions of tacrine and 3-(4-phenylbutoxy)-9*H*-xanthen-9-one (**23**) (carbon atoms are coloured green) with the adjacent amino residues (carbons atoms are purple) in AChE active site. Other atoms are coloured according to elements. (a) and (b) represent the docking results of the ligands to *Electrophorus electricus* AChE (PDB ID: 1C2O) while (c) and (d) represent the docking results of the ligands to human AChE (PDB ID: 4PQE).

Attempts to correlate the predicted CDOCKER binding energy with the AChE inhibitory activity were however unsuccessful. Thus, several scoring functions including LigScore1, LigScore2, PLP1, PLP2, Jain, PMF, PMF04 and Libdock score were explored further to quantify the interactions of compound **23** and tacrine with *Electrophorus electricus* AChE. Among the scoring functions, only the Jain score managed to give a positive correlation. The Jain score is a sum of five interaction terms including lipophilic interactions, polar attractive interactions, polar repulsive interactions, solvation of the protein and ligand, and an entropy term of the ligand[66]. According to the predicted Jain score, compound **23** is predicted to bind favourable to the human AChE. This suggests that this compound could potentially serve as a lead AChE inhibitor and may be further tested in the human enzyme model.

Conclusions

In summary, 3-hydroxyxanthone (**1**) and a series of twenty-nine new xanthone derivatives (**2**–**30**) were synthesised successfully by reacting **1** with seven different types of hydrocarbon substituents, including alkyl, alkenyl, alkynyl, alkylphenyl, ether, ester, and

hydroxyl groups. These xanthones possessed stronger anticholinergic activities towards AChE than BChE. Eleven xanthone derivatives were found to exhibit potent AChE inhibition effect with the IC_{50} values lower than 1.28 μM. SAR study revealed that hydrophobic interaction and hydrogen bonding of the substituent groups contribute to the inhibition effects, particularly the substituent group that is made up of saturated linear hydrocarbon with 4-carbons in the chain and preferably with an addition of phenyl or oxygenated group. Molecular docking study on **23** further confirmed the importance of the hydrophobic group as the side chain of these derivatives in the anti-AChE activities through π-π interactions in the active site, in addition to π–π stacking and hydrogen-bonding contributed by the xanthone main skeleton. The present work revealed that the new xanthone derivatives, particularly **23** and **28** are potent and selective AChE inhibitors that are potential lead compounds to be developed into anti-Alzheimer drug.

Disclosure statement

No potential conflict of interest was reported by the author(s).

Funding

The present work was financially supported by the Fundamental Research Grant Scheme (FRGS) [FRGS/1/2019/STG01/TAYLOR/02/1] from the Ministry of Education (MOE).

ORCID

Siau Hui Mah http://orcid.org/0000-0003-0370-4866

References

1. Prince M, Wimo A, Guerchet M, et al. World Alzheimer Report 2015: the global impact of dementia: an analysis of prevalence, incidence, cost and trends. Alzheimer's Dis Int 2015;17:2016.
2. Gaugler J, James B, Johnson T, et al. 2019 Alzheimer's disease facts and figures. Alzheimers & Dementia 2019;15: 321–87.
3. Lee YJ, Han SB, Nam SY, et al. Inflammation and Alzheimer's disease. Arch Pharm Res 2010;33:1539–56.
4. Association A. 2018 Alzheimer's disease facts and figures. Alzheimer's & Dementia 2018;14:367–429.
5. Luo L, Li Y, Qiang X, et al. Multifunctional thioxanthone derivatives with acetylcholinesterase, monoamine oxidases and β-amyloid aggregation inhibitory activities as potential agents against Alzheimer's disease. Bioorg Med Chem 2017; 25:1997–2009.
6. Gupta S, Mohan CG. 3D-pharmacophore model based virtual screening to identify dual-binding site and selective acetylcholinesterase inhibitors. Med Chem Res 2011;20:1422–30.
7. Zhao T, Ding K-M, Zhang L, et al. Acetylcholinesterase and butyrylcholinesterase inhibitory activities of β-carboline and quinoline alkaloids derivatives from the plants of genus *Peganum*. J Chem 2013;2013:1–6.
8. Woolf NJ. A structural basis for memory storage in mammals. Prog Neurobiol 1998;55:59–77.
9. Woolf NJ. Acetylcholine, cognition, and consciousness. J Mol Neurosci 2006;30:219–22.
10. Williams A, Zhou S, Zhan C-G. Discovery of potent and selective butyrylcholinesterase inhibitors through the use of pharmacophore-based screening. Bioorganic Med Chem Lett 2019;29:126754.
11. Kihara T, Shimohama S. Alzheimer's disease and acetylcholine receptors. Acta Neurobiol Exp (Wars) 2004;64:99–106.
12. Nordberg A, Svensson A-L. Cholinesterase inhibitors in the treatment of Alzheimer's disease: a comparison of tolerability and pharmacology. Drug Saf 1998;19:465–80.
13. Cheng ZQ, Zhu KK, Zhang J, et al. Molecular-docking-guided design and synthesis of new IAA-tacrine hybrids as multifunctional AChE/BChE inhibitors. Bioorg Chem 2019;83: 277–88.
14. Ballard C. Advances in the treatment of Alzheimer's disease: benefits of dual cholinesterase inhibition. Eur Neurol 2002; 47:64–70.
15. Khaw K, Choi S, Tan S, et al. Prenylated xanthones from mangosteen as promising cholinesterase inhibitors and their molecular docking studies. Phytomedicine 2014;21:1303–9.
16. Schneider LS. A critical review of cholinesterase inhibitors as a treatment modality in Alzheimer's disease. Dialogues Clin Neurosci 2000;2:111.
17. Ma W, Bi J, Zhao C, et al. Design, synthesis and biological evaluation of acridone glycosides as selective BChE inhibitors. Carbohydr Res 2020; 491:107977.
18. Brewster JT, Dell'Acqua S, Thach DQ, Sessler JL. Classics in chemical neuroscience: donepezil. ACS Chem Neurosci 2019; 10:155–67.
19. Razay G, Wilcock GK. Galantamine in Alzheimer's disease. Expert Rev Neurother 2008;8:9–17.
20. Jann MW. Rivastigmine, a new-generation cholinesterase inhibitor for the treatment of Alzheimer's disease. Pharmacotherapy: J Hum Drug Pharmacol ther 2000;20:1–12.
21. Trang A, Khandhar PB. Physiology, acetylcholinesterase. Tampa, FL: StatPearls Publishing; 2019.
22. Alzheimer's Disease Fact Sheet. National Institute on Aging. Available from: https://www.nia.nih.gov/health/alzheimers-disease-fact-sheet
23. Liu C, Zhang M, Zhang Z, et al. Synthesis and anticancer potential of novel xanthone derivatives with 3,6-substituted chains. Bioorg Med Chem 2016;24:4263–71.
24. Veeresham C. Natural products derived from plants as a source of drugs. J Adv Pharm Technol Res 2012;3:200–1.
25. Xia Z, Zhang H, Xu D, et al. Xanthones from the leaves of *Garcinia cowa* induce cell cycle arrest, apoptosis, and autophagy in cancer cells. Molecules 2015;20:11387–99.
26. Luo CT, Mao SS, Liu FL, et al. Antioxidant xanthones from *Swertia mussotii*, a high altitude plant. Fitoterapia 2013;91: 140–7.
27. Hashim NM, Rahmani M, Ee GCL, et al. Antioxidant, antimicrobial and tyrosinase inhibitory activities of xanthones isolated from *Artocarpus obtusus* FM Jarrett. Molecules 2012; 17:6071–82.
28. Dharmaratne H, Napagoda M, Tennakoon S. Xanthones from roots of *Calophyllum thwaitesii* and their bioactivity. Nat Prod Res 2009;23:539–45.
29. Auranwiwat C, Laphookhieo S, Rattanajak R, et al. Antimalarial polyoxygenated and prenylated xanthones from the leaves and branches of *Garcinia mckeaniana*. Tetrahedron 2016;72:6837–42.

30. Seo EJ, Curtis-Long MJ, Lee BW, et al. Xanthones from *Cudrania tricuspidata* displaying potent α-glucosidase inhibition. Bioorganic Med Chem Lett 2007;17:6421–4.
31. Zuo J, Ji CL, Xia Y, et al. Xanthones as α-glucosidase inhibitors from the antihyperglycemic extract of *Securidaca inappendiculata*. Pharm Biol 2014;52:898–903.
32. Urbain A, Marston A, Queiroz EF, et al. Xanthones from *Gentiana campestris* as new acetylcholinesterase inhibitors. Planta Med 2004;70:1011–4.
33. Zhang DD, Zhang H, Lao YZ, et al. Anti-inflammatory effect of 1,3,5,7-tetrahydroxy-8-isoprenylxanthone isolated from twigs of *Garcinia esculenta* on stimulated macrophage. Mediators Inflamm 2015;2015:350564.
34. Dzoyem JP, Lannang AM, Fouotsa H, et al. Anti-inflammatory activity of benzophenone and xanthone derivatives isolated from *Garcinia* (Clusiaceae) species. Phytochem Lett 2015;14: 153–8.
35. Chen LG, Yang LL, Wang CC. Anti-inflammatory activity of mangostins from *Garcinia mangostana*. Food Chem Toxicol 2008;46:688–93.
36. Bumrungpert A, Kalpravidh RW, Chuang CC, et al. Xanthones from mangosteen inhibit inflammation in human macrophages and in human adipocytes exposed to macrophage-conditioned media. J Nutr 2010;140:842–7.
37. Pedro M, Cerqueira F, Sousa ME, et al. Xanthones as inhibitors of growth of human cancer cell lines and their effects on the proliferation of human lymphocytes *in vitro*. Bioorg Med Chem 2002;10:3725–30.
38. Pinto M, Sousa M, Nascimento M. Xanthone derivatives: new insights in biological activities. Curr Med Chem 2005;12: 2517–38.
39. Ahmad I. Recent insight into the biological activities of synthetic xanthone derivatives. Eur J Med Chem 2016;116: 267–80.
40. Proença C, Albuquerque HM, Ribeiro D, et al. Novel chromone and xanthone derivatives: synthesis and ROS/RNS scavenging activities. Eur J Med Chem 2016;115:381–92.
41. Ellman GL, Courtney KD, Andres V, Feather-Stone RM. A new and rapid colorimetric determination of acetylcholinesterase activity. Biochem Pharmacol 1961;7:88–95.
42. Bairy PS, Das A, Nainwal LM, et al. Design, synthesis and anti-diabetic activity of some novel xanthone derivatives targeting α-glucosidase. Bangladesh J Pharmacol 2016;11: 308–18.
43. Fei X, Jo M, Lee B, et al. Synthesis of xanthone derivatives based on α-mangostin and their biological evaluation for anti-cancer agents. Bioorganic Med Chem Lett 2014;24: 2062–5.
44. Bruker. APEX2, SAINT and SADABS. Madison, WI: Bruker AXS Inc.; 2012.
45. Sheldrick GM. A short history of SHELX. A Short History of SHELX 2008;A64:112–22.
46. Sheldrick G. SHELXT – Integrated space-group and crystal-structure determination. AcCrA 2015;71:3–8.
47. Özkay ÜD, Can ÖD, Sağlık BN, et al. Design, synthesis, and AChE inhibitory activity of new benzothiazole–piperazines. Bioorganic Med Chem Lett 2016;26:5387–94.
48. Šinko G. Assessment of scoring functions and in silico parameters for AChE-ligand interactions as a tool for predicting inhibition potency. Chem Biol Interact 2019;308: 216–23.
49. Harel M, Schalk I, Ehret-Sabatier L, et al. Quaternary ligand binding to aromatic residues in the active-site gorge of acetylcholinesterase. Proc Natl Acad Sci 1993;90:9031–5.
50. Fernandes EG, Silva AM, Cavaleiro JA, et al. ^{1}H and ^{13}C NMR Spectroscopy of mono-, di-, tri-and tetrasubstituted xanthones. Magn Reson Chem 1998;36:305–9.
51. Zhang X, Li X, Ye S, et al. Synthesis, SAR and biological evaluation of natural and non-natural hydroxylated and prenylated xanthones as antitumor agents. Med Chem 2012;8: 1012–25.
52. Shrivastava SK, Srivastava P, Upendra T, et al. Design, synthesis and evaluation of some N-methylenebenzenamine derivatives as selective acetylcholinesterase (AChE) inhibitor and antioxidant to enhance learning and memory. Bioorg Med Chem 2017;25:1471–80.
53. Saenkham A, Jaratrungtawee A, Siriwattanasathien Y, et al. Highly potent cholinesterase inhibition of geranylated xanthones from *Garcinia fusca* and molecular docking studies. Fitoterapia 2020;146:104637.
54. Brühlmann C, Marston A, Hostettmann K, et al. Screening of non-alkaloidal natural compounds as acetylcholinesterase inhibitors . Chem Biodivers 2004;1:819–29.
55. Khan MTH, Orhan I, Senol FS, et al. Cholinesterase inhibitory activities of some flavonoid derivatives and chosen xanthone and their molecular docking studies. Chem Biol Interact 2009;181:383–9.
56. Urbain A, Marston A, Grilo LS, et al. Xanthones from *Gentianella amarella* ssp. acuta with acetylcholinesterase and monoamine oxidase inhibitory activities. J Nat Prod 2008;71: 895–7.
57. Cruz I, Puthongking P, Cravo S, et al. Xanthone and flavone derivatives as dual agents with acetylcholinesterase inhibition and antioxidant activity as potential anti-Alzheimer agents. J Chem 2017;2017:8587260.
58. Qin J, Lan W, Liu Z, et al. Synthesis and biological evaluation of 1,3-dihydroxyxanthone mannich base derivatives as anticholinesterase agents. Chem Cent J 2013;7:78.
59. Piazzi L, Belluti F, Bisi A, et al. Cholinesterase inhibitors: SAR and enzyme inhibitory activity of 3-[omega-(benzylmethylamino)alkoxy]xanthen-9-ones. Bioorg Med Chem 2007;15: 575–85.
60. Imramovsky A, Stepankova S, Vanco J, et al. Acetylcholinesterase-inhibiting activity of salicylanilide N-alkylcarbamates and their molecular docking. Molecules 2012;17:10142–58.
61. Bagheri SM, Khoobi M, Nadri H, et al. Synthesis and anticholinergic activity of 4-hydroxycoumarin derivatives containing substituted benzyl-1,2,3-triazole moiety. Chem Biol Drug Des 2015;86:1215–20.
62. Banks WA. Characteristics of compounds that cross the blood-brain barrier. BMC Neurol 2009;9:S3.
63. Dong X. Current strategies for brain drug delivery. Theranostics 2018;8:1481–93.
64. Nachon F, Carletti E, Ronco C, et al. Crystal structures of human cholinesterases in complex with huprine W and tacrine: elements of specificity for anti-Alzheimer's drugs targeting acetyl-and butyryl-cholinesterase. Biochem J 2013; 453:393–9.
65. Cheung J, Rudolph MJ, Burshteyn F, et al. Structures of human acetylcholinesterase in complex with

pharmacologically important ligands. J Med Chem 2012; 55:10282–6.

66. Jain AN. Scoring noncovalent protein-ligand interactions: a continuous differentiable function tuned to compute binding affinities. J Comput Aided Mol Des 1996;10:427–40.